10.1071/CH14422_AC

Australian Journal of Chemistry 2015, 68 (6), 970-980

SUPPLEMENTARY MATERIAL FOR:

$Cu(hfac)_2$ Complexes with Nitronyl Ketones Structurally Mimicking Nitronyl Nitroxides in Breathing Crystals

Evgeny V. Tretyakov,[A] *Galina V. Romanenko,*[A] *Sergey L. Veber,*[A,B] *Matvey V. Fedin,*[A,B] *Aleksey V. Polushkin,*[A] *Anastasia O. Tkacheva,*[A] *and Victor I. Ovcharenko*[A,C]

[A] International Tomography Center, Siberian Branch of the Russian Academy of Sciences, Institutskaya str. 3a, 630090 Novosibirsk, Russian Federation.

[B] Novosibirsk State University, Pirogova str. 2, 630090 Novosibirsk, Russian Federation.

[C] Corresponding author. Email: Victor.Ovcharenko@tomo.nsc.ru

Contents **Page**

1. Data of X-ray Analysis for **4a,b**, **13c,d** and **14b,c** S2

2. Structural Dynamics of $[Cu(hfac)_2\mathbf{NN^{Me}}]_n$ and α-$[Cu(hfac)_2(\mathbf{4a})]_n$ S5

3. Data of X-ray Analysis for Chain Complexes
β-$[Cu(hfac)_2(4a)]_n$, $[Cu(hfac)_2(4c)]_n$, and $[Cu(hfac)_2(4d)]_n$ S6

4. Data of X-ray Analysis for Molecular Complexes $[Cu(hfac)_2(\mathbf{4a})_2]$, $[Cu(hfac)_2(\mathbf{4b})]$, $[(Cu(hfac)_2)_3(\mathbf{4c})_2]$, $[Cu(hfac)_2(\mathbf{4c})]$, and $[(Cu(hfac)_2)_3(\mathbf{4d})_2]$ S8

5. Supplementary EPR data S12

6. Supplementary FTIR data S15

7. ^1H, ^{13}C NMR, IR and Mass Spectra S18

8. IR Spectra of $\mathbf{NN^{Alk}}$, and Comparison of IR Spectra of $\mathbf{NN^{Alk}}$ (Alk = Me, Et) and **4a,b** S47

Data of X-ray Analysis for 4a,b, 13c,d and 14b,c

In molecules **13c,d**, the bond lengths are typical for all of their functional groups. We notice that the length of the alkyl substituent in the pyrazole ring appreciably affects the conformation of molecules **13c** and **13d** in crystal.

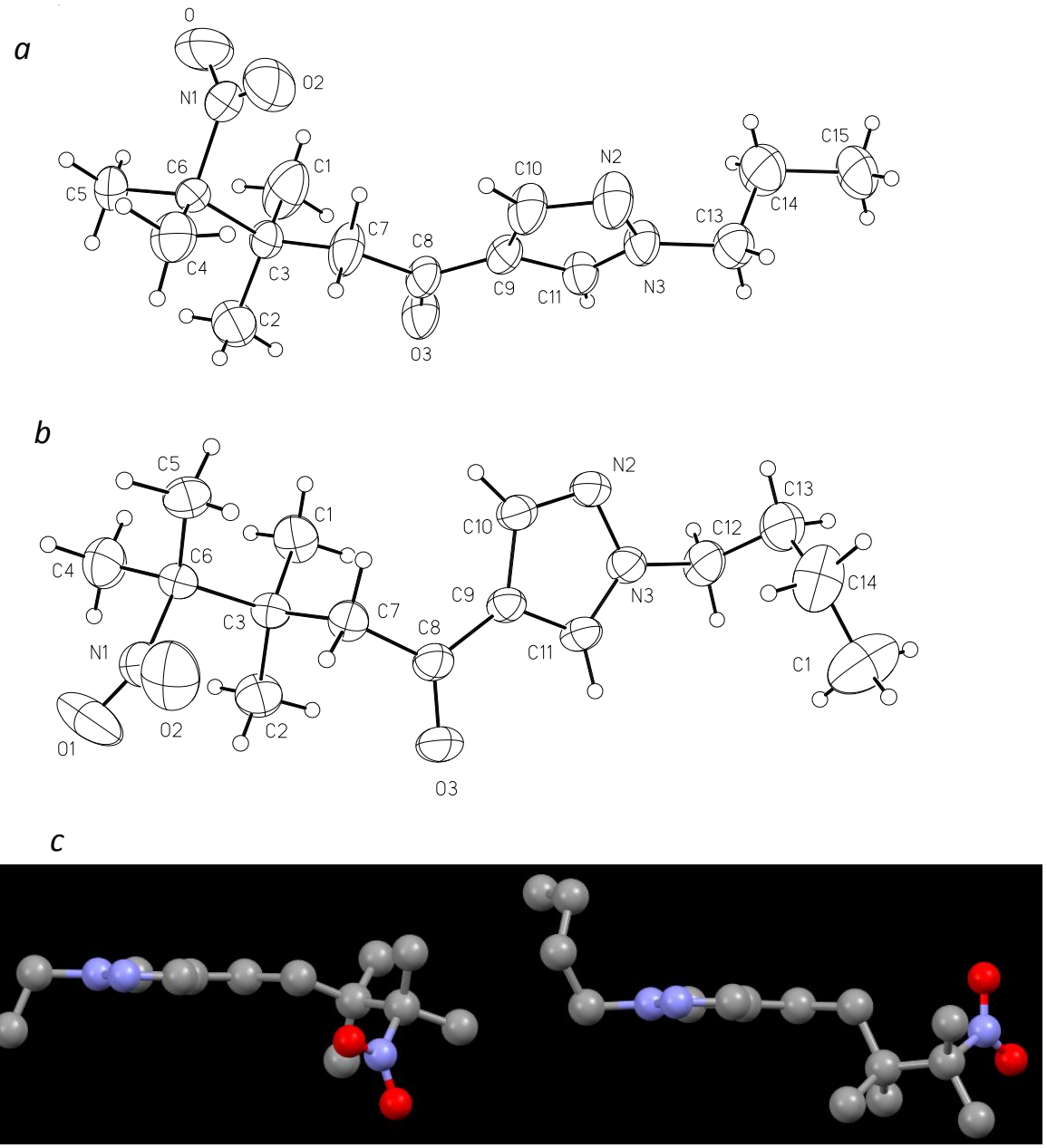

Fig. S1. *ORTEP* diagram derived from the single-crystal X-ray analysis of **13c** (*a*) and **13d** (*b*), and the difference in their conformations (*c*).

Nitrone **14b** crystallizes in the monoclinic space group $P2_1/c$ with two crystallographically independent molecules having almost the same geometry. The structure of **14c** contains crystallization water molecules, which bind two neighboring molecules into centrosymmetric dimers via N…H–O–H…O hydrogen bonds involving the N atoms of the pyrazole rings and the O atoms of the nitrone group. The increase in the N–O distance in **14c** (1.313(5) Å versus 1.303(1) and 1.293(1) Å in **14b**) is probably related to the participation of the NO group in H-bonding.

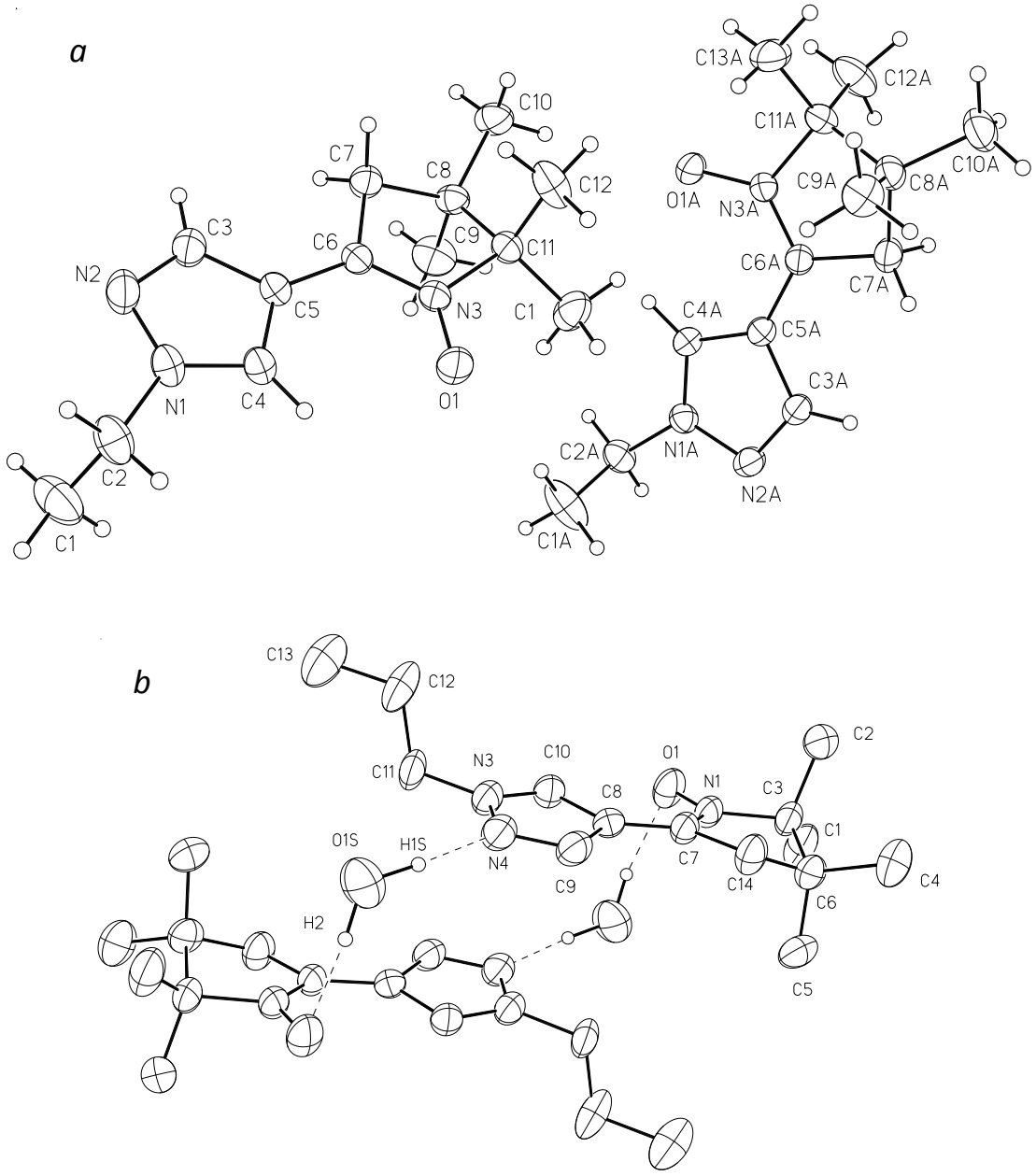

Fig. S2. *ORTEP* diagram derived from the single-crystal X-ray analysis of **14b** (*a*) and **14c**·$\mathbf{H_2O}$ (*b*, H atoms of **14c** are omitted).

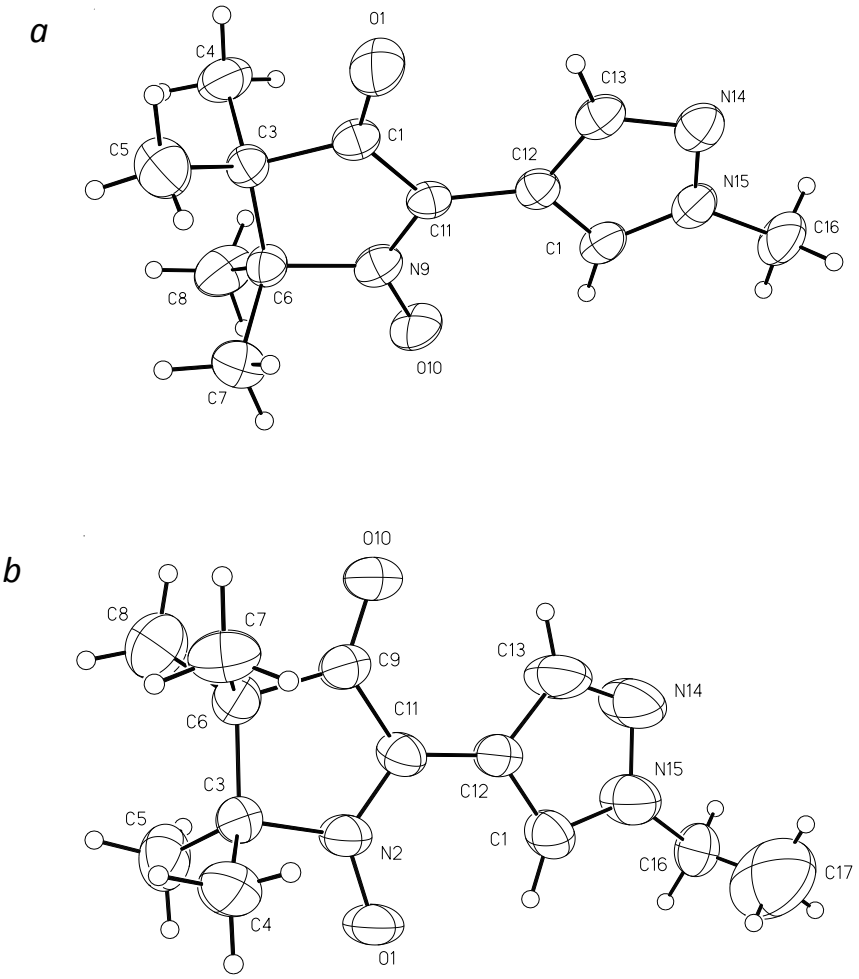

Fig. S3. *ORTEP* diagram derived from the single-crystal X-ray analysis of the nitronyl ketones **4a-1** (*a*) and **4b** (*b*). Hydrogen atoms are drawn as circles with small radii.

Table S1. Selected geometrical characteristics of nitronyl ketones **4a,b** in comparison with those for the nitronyl nitroxides **NN^{Me}** and **NN^{Et}**

	4a-1	**4a-2** [A]	**NN^{Me}** [B]	**4b**	**NN^{Et}** [D]
C-C (between rings)	1.447(5)	1.434(2)	1.427(3)	1.443(3)	1.422(4)
N–O	1.281(3)	1.260(1)	1.278(3) 1.282(2)	1.266(3)	1.294(3) 1.292(3)
C=O	1.240(4)	1.251(1)	–	1.223(3)	–
C(11)–C(9)	1.409(4)	1.391(2)	–	1.432(3)	–
C(11)–N	1.337(4)	1.372(2)	1.347(2) 1.342(2)	1.319(3)	1.336(3) 1.330(3)
∠{CNO}–Pz	4.58	3.62	3.44	0.00	5.14
N–O…O–X [C]	3.458(3)	4.706(2)	4.608(2)	3.819(4)	4.041(3)

[A] In modification **4a-2**, the O=C-C=N$^+$-O$^-$ molecular fragment is disordered (the statistical weights of the C=O and N–O groups are equal, 0.45 and 0.55, respectively).

[B] See reference: S. Fokin, V. Ovcharenko, G. Romanenko, V. Ikorskii, *Inorg. Chem*. **2004**, *43*, 969.

[C] Intermolecular distances N–O…O–N in **NN^{Alk}** or N–O…O=C in **4a,b**. [D] This work.

Table S2. Selected structural parameters (bond lengths/Å, angle/°) in [Cu(hfac)$_2$**NN^{Me}**]$_n$ and α-[Cu(hfac)$_2$(**4a**)]$_n$ at different temperatures [A]

T, K	L	**295** (295 [B])	**240** (240 [B])	**150** (160 [C])	**105** (120 [B])
Cu–O$_{hfac}$	**4a**	**1.937(2)–1.959(2)**	**1.942(2)–1.960(2)**	**1.940(3)–1.957(3)**	**1.947(2)–1.964(2)**
	NN^{Me}	1.933(2)–1.963(2)	1.948(3)–1.974(3)	1.939(2)–1.978(2)	1.941(7)–2.010(9) 2.250(8) 2.288(7)
Cu–O$_{NO}$	**4a**	**2.581(3)**	**2.634(2), 2.580(2)**	**2.619(3), 2.550(3)**	**2.613(3), 2.545(3)**
	NN^{Me}	2.476(3)	2.491(4), 2.494(4)	2.480(2), 2.479(2)	1.991(7), 2.448(8)
Cu–N	**4a**	**2.277(3)**	**2.228(2), 2.295(2)**	**2.280(3), 2.283(3)**	**2.289(3), 2.284(3)**
	NN^{Me}	2.308(3)	2.302(4), 2.318(4)	2.301(2), 2.304(2)	2.004(9), 2.34(1)
∠CuO$_{NO}$N	**4a**	**146.9(2)**	**132.4(2), 157.0(2)**	**131.4(3), 158.5(3)**	**130.9(2), 158.0(3)**
	NN^{Me}	139.8(2)	128.5(3), 151.1(4)	128.1(1), 151.7(2)	125.9(6), 150.9(6)
N–O$_{Cu}$	**4a**	**1.260(3)**	**1.259(3), 1.272(3)**	**1.277(4), 1.276(4)**	**1.271(4), 1.273(4)**
	NN^{Me}	1.288(4)	1.282(5), 1.290(5)	1.288(3), 1.292(3)	1.31(1), 1.27(1)
C=O/N–O	**4a**	**1.229(4)**	**1.225(3), 1.218(3)**	**1.226(5), 1.225(5)**	**1.221(4), 1.222(4)**
	NN^{Me}	1.278(4)	1.274(5), 1.269(6)	1.277(3), 1.270(3)	1.27(1), 1.27(2)

[A] Temperatures (K) of XRD experiments for **[Cu(hfac)$_2$NN^{Me}]$_n$** are given in brackets.

[B] See reference: V. I. Ovcharenko, K. Yu. Maryunina, S. V. Fokin, E. V. Tretyakov, G. V. Romanenko, V. N. Ikorskii, *Russ. Chem. Bull*. **2004**, *53*, 2406.

[C] This work.

Data of X-ray Analysis for Chain Complexes β-[Cu(hfac)$_2$(4a)]$_n$, [Cu(hfac)$_2$(4c)]$_n$, and [Cu(hfac)$_2$(4d)]$_n$

The bond lengths and valence angle values in chains of α- and β-[Cu(hfac)$_2$(**4a**)]$_n$ are almost the same equal, with the exception of the angle at O atom of coordinated NO group (Table S3). But the packing of chains are quite different: in case of α-modification the chains, connected by the inversion center, lie in parallel layers, in the β-modification chains in the neighboring layers are perpendicular (Figure S4).

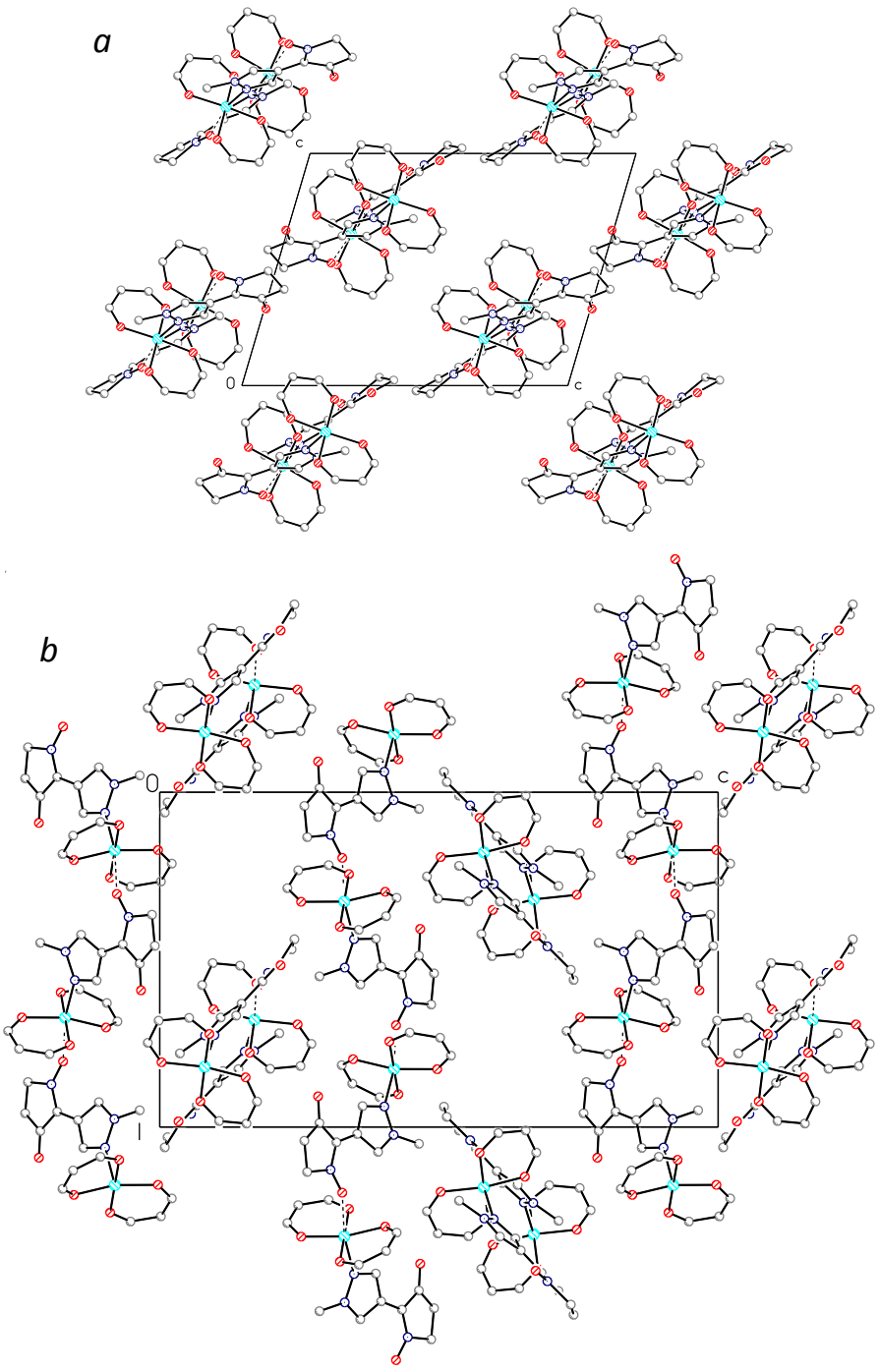

Fig. S4. Chain packing in the structures of α- (*a*) and β-[Cu(hfac)$_2$(**4a**)]$_n$ (*b*).

Table S3. Selected bond lengths (Å) and angle (º) in α-[Cu(hfac)$_2$(**4a**)]$_n$ and β-[Cu(hfac)$_2$(**4a**)]$_n$.

	α-[Cu(hfac)$_2$(**4a**)]$_n$	β-[Cu(hfac)$_2$(**4a**)]$_n$
T (K)	295	295
Cu–O$_{hfac}$	1.937(2)–1.959(2)	1.951(3)–1.970(3)
Cu–O$_{NO}$	2.581(3)	2.591(4)
Cu–N	2.277(3)	2.271(3)
N–O	1.260(3)	1.262(5)
C–O	1.229(4)	1.220(6)
∠Cu–O–N	146.9(2)	152.8(4)

Structures of the polymer chains in complexes [Cu(hfac)$_2$(**4c**)]$_n$ and [Cu(hfac)$_2$(**4d**)]$_n$ (Fig. S5, Table S4) are the same as those in [Cu(hfac)$_2$(**4a**)]$_n$ (see the main text).

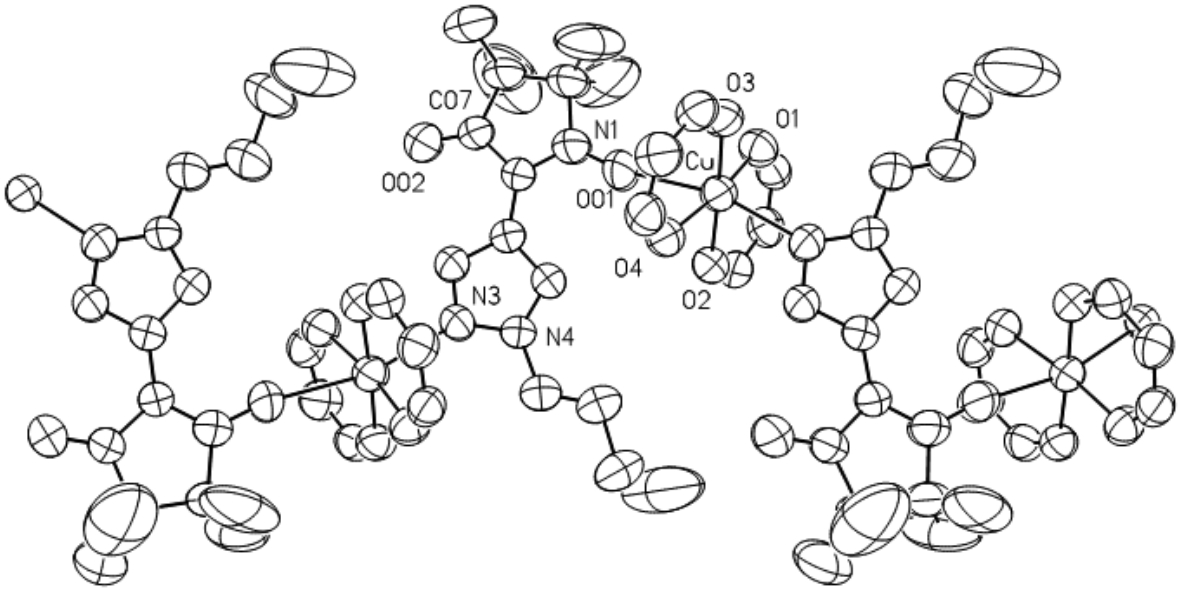

Fig. S5. The fragment of chain in [Cu(hfac)$_2$(**4d**)]$_n$.

Table S4. Selected bond lengths (Å) and angle (º) in [Cu(hfac)$_2$(**4c**)]$_n$ and [Cu(hfac)$_2$(**4d**)]$_n$.

	[Cu(hfac)$_2$(**4c**)]$_n$		[Cu(hfac)$_2$(**4d**)]$_n$
T (K)	295	105	295
Cu–O$_{hfac}$	1.941(3)–1.957(3)	1.949(3)–1.973(3)	1.944(3)–1.957(3)
Cu–O$_{NO}$	2.530(4)	2.458(3)	2.509(3)
Cu–N	2.345(4)	2.336(3)	2.342(3)
N–O	1.264(5)	1.255(5)	1.250(4)
C–O	1.245(6)	1.220(6)	1.221(5)
∠Cu–O–N	155.3(4)	159.3(3)	159.5(4)

Data of X-ray Analysis for Molecular Complexes $[Cu(hfac)_2(4a)_2]$, $[Cu(hfac)_2(4b)]$, $[Cu(hfac)_2(4c)]$, $[(Cu(hfac)_2)_3(4c)_2]$, and $[(Cu(hfac)_2)_3(4d)_2]$

The only isolated complex of $Cu(hfac)_2$ with **4b** has molecular structure (Fig. S6). In the complex, the Cu atom is surrounded by donor atoms forming a square pyramid, where one O_{hfac} atom is at the apex (Cu–O 2.200(2) Å), and the other three O_{hfac} atoms (Cu–O 1.920(2)–1.969(2) Å) and the N atom of the pyrazole ring (Cu–N 2.016(3) Å) at the base. The intermolecular distance Cu–O(1R') is equal to 2.982(2) Å, therefore formally $[Cu(hfac)_2(\mathbf{4b})]$ can be viewed as splitted "head-to-tail" chain. In complex $[Cu(hfac)_2(\mathbf{4b})]$, the $O{=}C\text{-}C{=}N^+\text{-}O^-$ fragment is disordered with the statistical weights of the C=O and N–O groups equal 0.5. For this reason XRD experiments give practically equal C=O and N–O distances: 1.246(3) and 1.253(4) Å, respectively.

Molecular complex $[Cu(hfac)_2(\mathbf{4c})]$, prepared by interaction of two equivalents of $[(Cu(hfac)_2)_3(\mathbf{4c})_2]$ and three equivalents of **4c** in hexane, has the same structure as $[Cu(hfac)_2(\mathbf{4b})]$: Cu–O 1.926(3)–1.959(3) Å, Cu–N 2.005(3) Å, Cu–O 2.201(3) Å, C=O/N–O – 1.243(4) и 1.247(5) Å, and intermolecular distance Cu–O(1R') 3.037(3) Å.

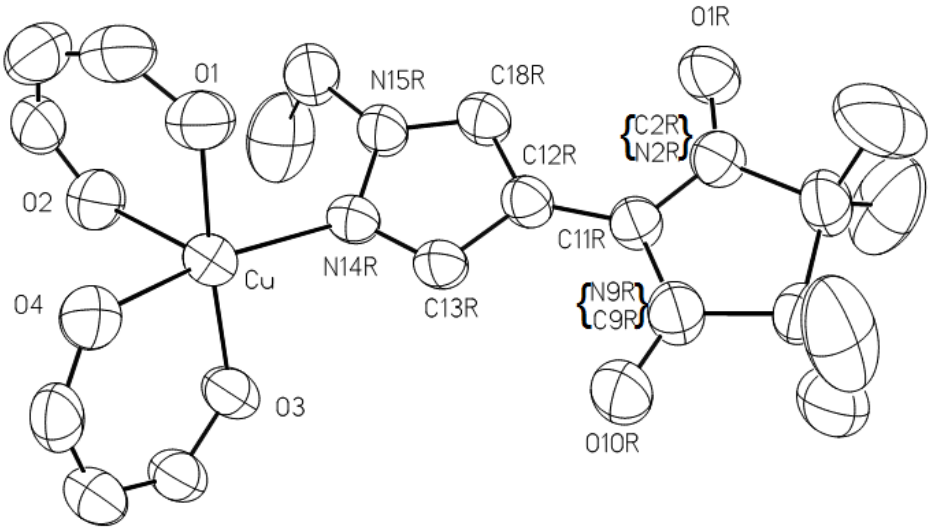

Fig. S6. Structure of the molecular complex $[Cu(hfac)_2(\mathbf{4b})]$.

Molecular centrosymmetric complexes [(Cu(hfac)$_2$)$_3$(**4c**)$_2$] and [(Cu(hfac)$_2$)$_3$(**4d**)$_2$] have similar structures (Fig. S7). In both complexes the central Cu atom has a square bypiramidal environment with O_{hfac} atoms forming an equatorial plane (Cu–O 1.930(2)–1.951(2) Å) and two O_{NO} atoms lying at the apexes of the polyhedron at distances of 2.401(2) and 2.410(3) Å in [(Cu(hfac)$_2$)$_3$(**4c**)$_2$] and [(Cu(hfac)$_2$)$_3$(**4d**)$_2$] correspondingly. The terminal Cu atoms have square pyramidal surroundings with the N atom of pyrazole ring in the apex (Cu–N 2.209(2) and 2.202(3) Å in [(Cu(hfac)$_2$)$_3$(**4c**)$_2$] and [(Cu(hfac)$_2$)$_3$(**4d**)$_2$] correspondingly) and O_{hfac} atoms (1.938(2)–1.964(2) Å) lying at the base of the pyramid (Cu–O 1.938(2)–1.964(2) Å). In complexes with **4c** and **4d**, the distances N–O are equal 1.268(2) and 1.268(4) Å, C=O - 1.218(2) and 1.223(4) Å, respectively.

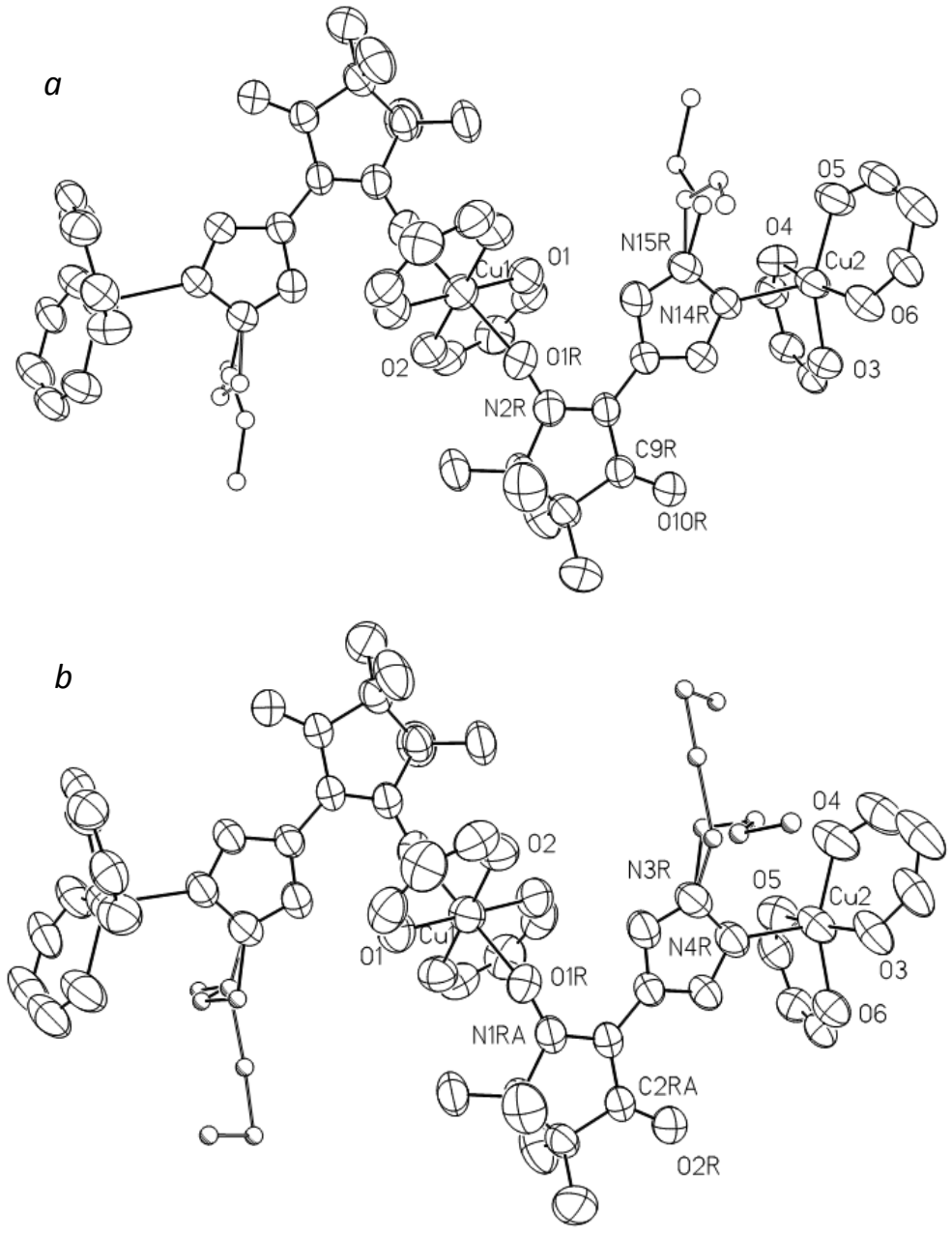

Fig. S7. Structure of the molecular complexes [(Cu(hfac)$_2$)$_3$(**4c**)$_2$] (*a*) and [(Cu(hfac)$_2$)$_3$(**4d**)$_2$ (*b*).

Complex [Cu(hfac)$_2$(**4a**)$_2$] is molecular (Fig. S8). The centrosymmetric environment of the Cu atom is the flattened octahedron characterized by short axial distance Cu–O(1) (1.949(4) Å) and rather long equatorial distances Cu–N(14R) and Cu–O(2) (2.132(6) and 2.183(5) Å, respectively). In **4a** N(9R)–O(10R) and O(1R)–C(2R) bond lengths are equal to 1.271(11) and 1.232(10) Å.

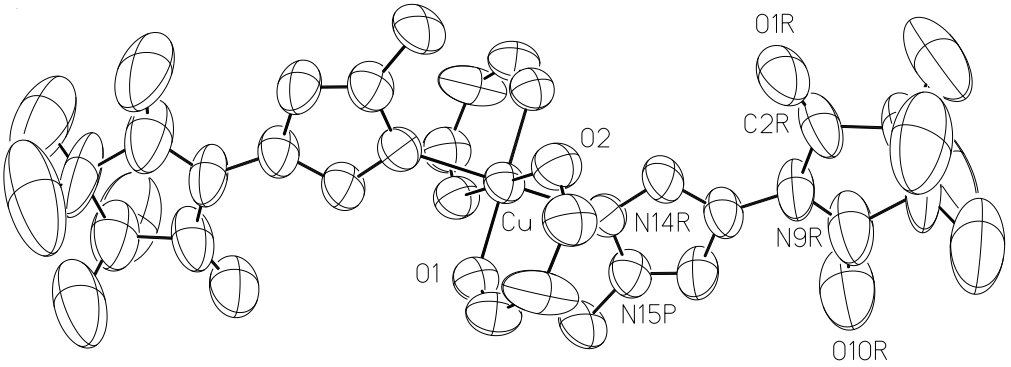

Fig. S8. Structure of the molecular complex [Cu(hfac)$_2$(**4a**)$_2$].

*Crystallographic data for [Cu(hfac)$_2$(**4a**)$_2$], [(Cu(hfac)$_2$)$_3$(**4c**)$_2$], [(Cu(hfac)$_2$)$_3$(**4d**)$_2$], [Cu(hfac)$_2$(**4b**)], [Cu(hfac)$_2$(**4c**)], β-[Cu(hfac)$_2$(**4a**)]$_n$, and [Cu(hfac)$_2$(**NN^{Me}**)]*

[Cu(hfac)$_2$(**4a**)$_2$]: $C_{34}H_{36}CuF_{12}N_6O_8$, FW = 948.23, T = 240 K, monoclinic, $C2/c$, a = 29.064(3), b = 11.3429(13), c = 14.6069(14) Å, β = 116.830(7)°, V = 4297.0(8) Å^3, Z = 4, D_{calc} = 1.466 g/cm^3, μ(Mo Kα) = 0.613 mm^{-1}, a total of 18191 (θ_{max} = 28.38°), 5306 unique (R_{int} = 0.1527), 1171 ($F > 4\sigma_F$), 314 parameters, $Goof$ = 0.729, $R1$ = 0.0661, $wR2$ = 0.1428 ($I > 2\sigma_I$), $R1$ = 0.2041, $wR2$ = 0.2996 (all data), max / min diff. peak 0.362 / -0.563 eÅ^{-3}.

[(Cu(hfac)$_2$)$_3$(**4c**)$_2$]: $C_{58}H_{48}Cu_3F_{36}N_6O_{16}$, FW = 1959.64, T = 295 K, triclinic, P-1, a = 11.5684(5), b = 13.5059(6), c = 13.9175(6) Å, α = 73.938(2), β = 77.805(2), γ = 80.693(2)°, V = 2030.07(16) Å^3, Z = 1, D_{calc} = 1.603 g/cm^3, μ(Cu Kα) = 2.241 mm^{-1}, a total of 24380 (θ_{max} = 66.469°), 7034 unique (R_{int} = 0.0771), 6285 ($F > 4\sigma_F$), 728 parameters, $Goof$ = 1.009, $R1$ = 0.0507, $wR2$ = 0.1440 ($I > 2\sigma_I$), $R1$ = 0.0536, $wR2$ = 0.1489 (all data), max / min diff. peak 0.337 / -0.452 eÅ^{-3}.

[(Cu(hfac)$_2$)$_3$(**4d**)$_2$]: $C_{60}H_{52}Cu_3F_{36}N_6O_{16}$, FW = 1987.70, T = 295 K, triclinic, P-1, a = 11.492(2), b = 13.408(3), c = 14.048(3) Å, α = 77.32(3), β = 79.40(3), γ = 82.72(3)°, V = 2067.2(8) Å^3, Z = 1, D_{calc} = 1.597 g/cm^3, μ(Mo Kα) = 0.907 mm^{-1}, a total of 37594 (θ_{max} = 28.33°), 10201 unique (R_{int} = 0.0357), 4942 ($F > 4\sigma_F$), 700 parameters, $Goof$ = 0.998, $R1$ = 0.0589, $wR2$ = 0.1716 ($I > 2\sigma_I$), $R1$ = 0.1278, $wR2$ = 0.2181 (all data), max / min diff. peak 0.419 / -0.446 eÅ^{-3}.

[Cu(hfac)$_2$(**4b**)]: $C_{23}H_{21}CuF_{12}N_3O_6$, FW = 726.97, T = 295 K, monoclinic, $P2_1/c$, a = 12.0724(13), b = 29.156(3), c = 8.4518(10) Å, β = 99.002(7)°, V = 2938.3(6) Å^3, Z = 4, D_{calc} = 1.643 g/cm^3, μ(Cu Kα) = 2.161 mm^{-1}, a total of 15235 (θ_{max} = 57.49°), 3894 unique (R_{int} = 0.0704), 3001 ($F > 4\sigma_F$), 514 parameters, $Goof$ = 1.019, $R1$ = 0.0451, $wR2$ = 0.1239 ($I > 2\sigma_I$), $R1$ = 0.0588, $wR2$ = 0.1317 (all data), max / min diff. peak 0.309 / -0.343 eÅ^{-3}.

[Cu(hfac)$_2$(**4c**)]: $C_{24}H_{23}CuF_{12}N_3O_6$, FW = 740.99, T = 295 K, monoclinic, $P2_1/c$, a = 11.9943(4), b = 28.3710(12), c = 8.8243(3) Å, β = 99.690(2)°, V = 2959.98(19) Å^3, Z = 4, D_{calc} = 1.663 g/cm^3, μ(Cu Kα) = 2.157 mm^{-1}, a total of 15229 (θ_{max} = 66.84°), 4856 unique (R_{int} = 0.0619), 3414 ($F > 4\sigma_F$), 523 parameters, $Goof$ = 1.063, $R1$ = 0.0625, $wR2$ = 0.1862 ($I > 2\sigma_I$), $R1$ = 0.0905, $wR2$ = 0.2072 (all data), max / min diff. peak 0.662 / -0.524 eÅ^{-3}.

β-[Cu(hfac)$_2$(**4a**)]$_n$: $C_{22}H_{19}CuF_{12}N_3O_6$, FW = 712.94, T = 295 K, tetragonal, $P4_32_12$, a = 15.1970(7), c = 25.3326(13) Å, V = 5850.5(6) Å^3, Z = 8, D_{calc} = 1.619 g/cm^3, μ(Cu Kα) = 2.158 mm^{-1}, a total of 68155 (θ_{max} = 67.885°), 5274 unique (R_{int} = 0.0484), 5126 ($F > 4\sigma_F$), 424 parameters, $Goof$ = 1.072, $R1$ = 0.0442, $wR2$ = 0.1364 ($I > 2\sigma_I$), $R1$ = 0.0448, $wR2$ = 0.1374 (all data), max / min diff. peak 0.473 / -0.269 eÅ^{-3}.

[Cu(hfac)$_2$(**NN^{Me}**)]$_n$: $C_{21}H_{19}Cu_3F_{12}N_4O_6$, FW = 714.94, T = 160 K, triclinic, P-1, a = 12.1072(7), b = 15.4007(8), c = 15.9259(9) Å, α = 84.207(2), β = 74.161(2), γ = 87.545(2)°, V = 2841.8(3) Å^3, Z = 4, D_{calc} = 1.671 g/cm^3, μ(Cu Kα) = 2.233 mm^{-1}, a total of 27389 (θ_{max} = 67.43°), 9981 unique (R_{int} = 0.0322), 8983 ($F > 4\sigma_F$), 865 parameters, $Goof$ = 1.011, $R1$ = 0.0443, $wR2$ = 0.1248 ($I > 2\sigma_I$), $R1$ = 0.0483, $wR2$ = 0.1288 (all data), max / min diff. peak 0.755 / -0.467 eÅ^{-3}.

Supplementary EPR Data

Figures S9 and S10 show similar data as those in Fig.8 (main text) for compounds [Cu(hfac)$_2$(**4c**)]$_n$ and [Cu(hfac)$_2$(**4d**)]$_n$. These spectra show exactly the same trends as those of α-[Cu(hfac)$_2$(**4a**)]$_n$. Similar to α-[Cu(hfac)$_2$(**4a**)]$_n$, no indications of structural rearrangements (Jahn-Teller axis flips) are found for [Cu(hfac)$_2$(**4c**)]$_n$ and [Cu(hfac)$_2$(**4d**)]$_n$.

In addition to the above solid conclusions, we note that the shapes of the EPR spectra at some orientations are puzzling. We observe the two groups of copper signals that are clearly separated at certain angles and can be assigned to the two different types of copper ions in the polymer chains. However, for example the spectra of [Cu(hfac)$_2$(**4d**)]$_n$ (Fig. S10) at angles 80 or 140^0 show more complicated patterns with larger number of hyperfine splittings observed than expected for two types of copper ions. Since hyperfine splittings are clearly observed, the influence of exchange interaction between copper(II) ions can be neglected and observation of more than two nonequivalent copper(II) centers needs explanation. A puzzling number of hyperfine splittings is found close to the $g_{||}$ region where EPR spectrum is very sensitive to orientation of copper octahedron toward magnetic field (see Figs S9b and S10b for example). Knowing the elasticity of breathing crystals and flexibility of their polymer chains (and expecting the same for their ketone-containing analogs), the above observations can be rationalized if copper centers randomly occupy several alternative close orientations in the crystal lattice that differ by less than ~5^0 and thus may be indiscernible by XRD. Alternatively, if Cu–O distances in copper(II) centers are slightly different, the values of $g_{||}$ will also be different, and in the sensitive $g_{||}$ region the corresponding spectra can be shifted resulting in more EPR lines observed than expected. Thus, EPR data implies a set of slightly different conformations of copper(II) centers in [Cu(hfac)$_2$(**4d**)]$_n$ (and possibly two other complexes).This effect is very subtle and can be studied in more detail using high-field EPR; however, in general, it has no influence on important conclusions made above and could not hinder the observation of structural rearrangements if they would occur.

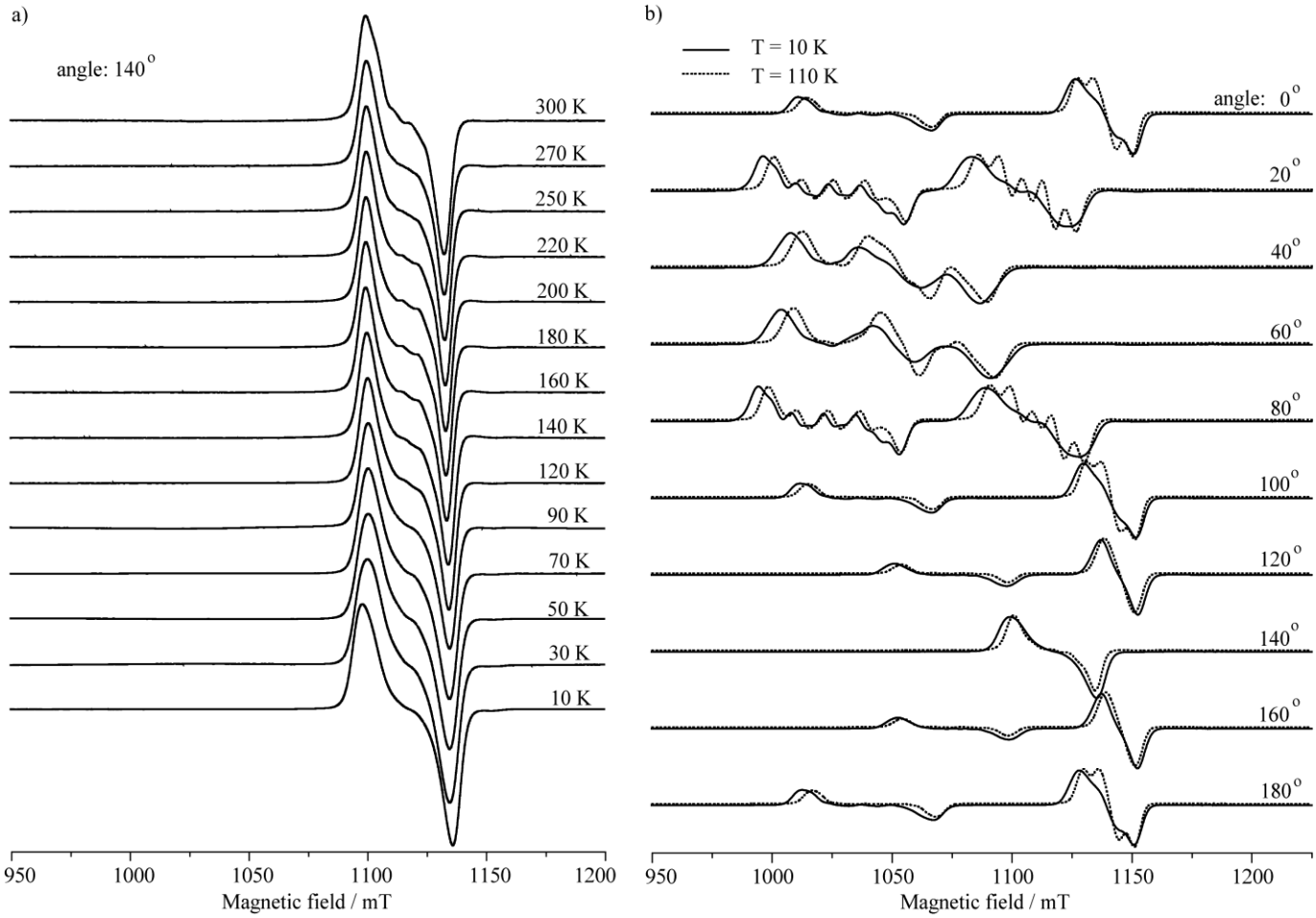

Figure S9. Q-band single-crystal EPR spectra of $[Cu(hfac)_2(\mathbf{4c})]_n$ at T = 10–300 K (ν_{mw}≈33.24 GHz, arbitrary crystal orientation). (a) Spectra at fixed angle vs. temperature. (b) Spectra collected at 10 and 110 K (solid and dashed lines, respectively) vs. angle.

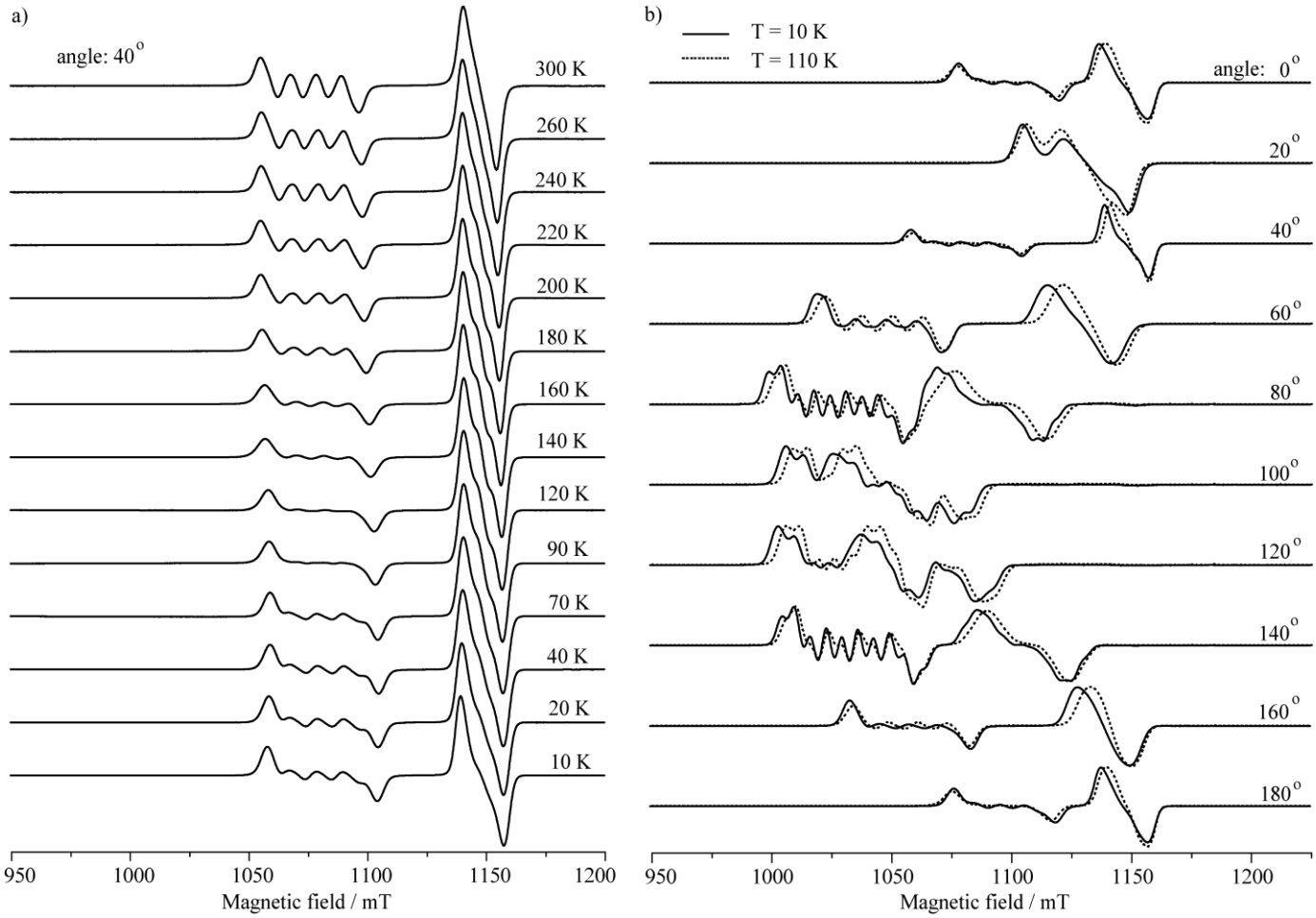

Figure S10. Q-band single-crystal EPR spectra of [Cu(hfac)$_2$(**4d**)]$_n$ at T = 10–300 K (ν_{mw}≈33.24 GHz, arbitrary crystal orientation). (a) Spectra at fixed angle vs. temperature. (b) Spectra collected at 10 and 110 K (solid and dashed lines, respectively) vs. angle.

Supplementary FTIR Data

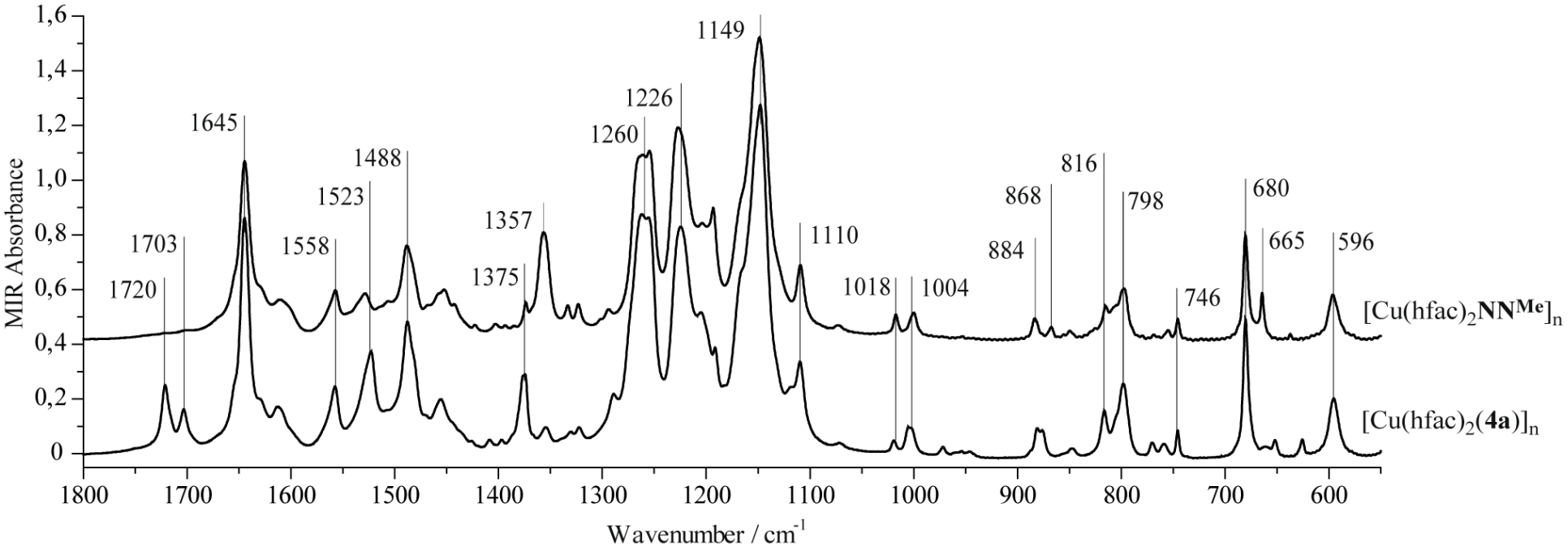

Figure S11. FTIR spectra of pellets of [Cu(hfac)$_2$**NN^{Me}**]$_n$ and its ketone-containing analog α-[Cu(hfac)$_2$(**4a**)]$_n$ measured at 300 K.

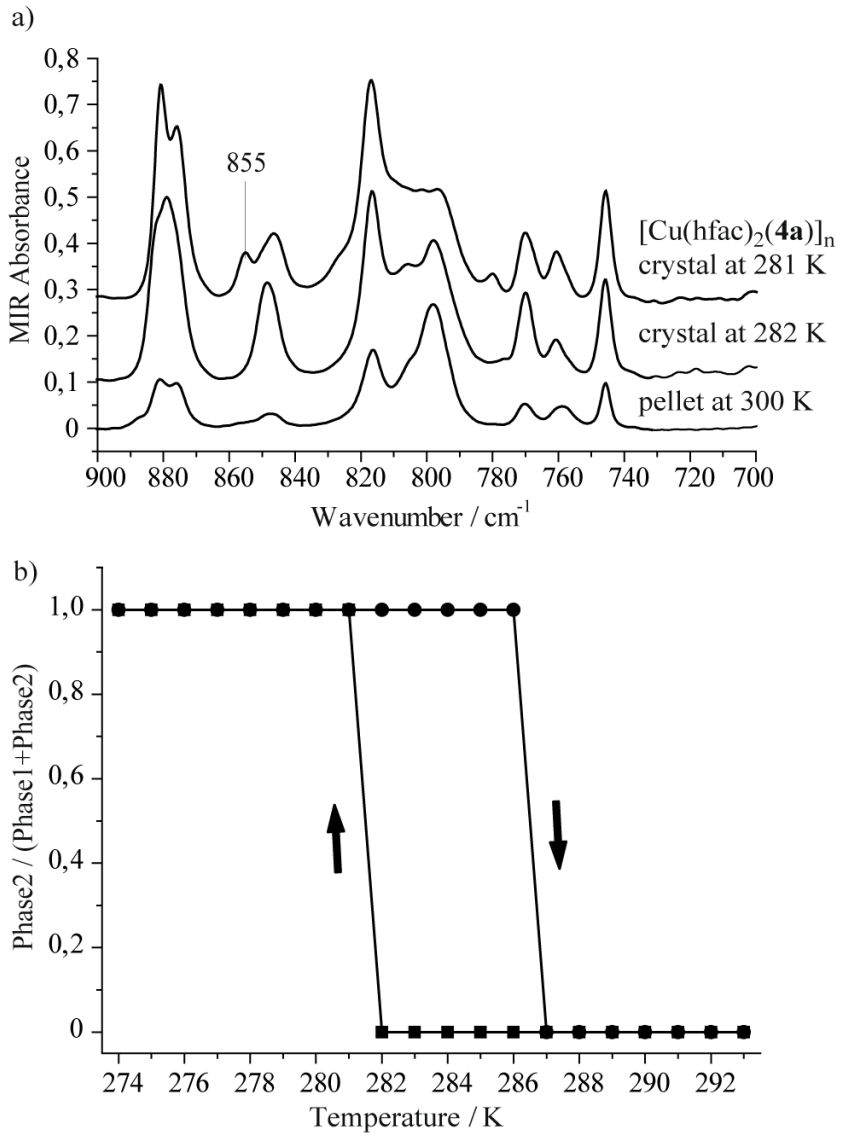

Figure S12. (a) FTIR spectra of α-[Cu(hfac)$_2$**(4a)**]$_n$ (single crystal) at 282 and 281 K obtained upon lowering of the temperature. Pellet spectrum at 300 K is shown for comparison. Absorption band at 855 cm^{-1} is selected for monitoring the hysteresis loop. (b) Hysteresis loop obtained for α-[Cu(hfac)$_2$**(4a)**]$_n$ (single crystal). Phase 2 corresponds to the low-temperature (triclinic) geometry, whereas Phase 1 corresponds to the high-temperature (monoclinic) geometry. Arrows indicate the direction of the temperature change.

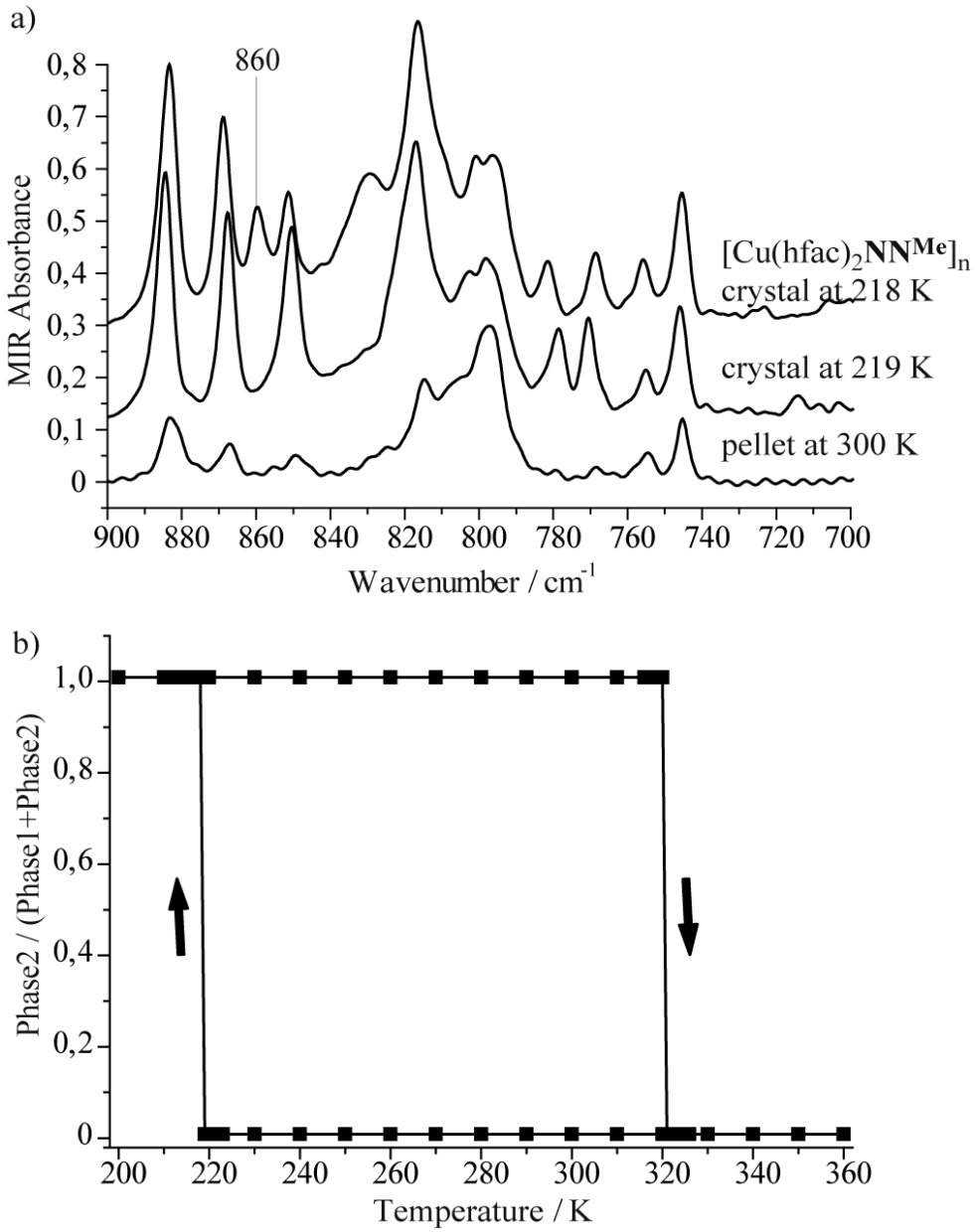

Figure S13. (a) FTIR spectra of [Cu(hfac)$_2$**NN^{Me}**]$_n$ (single crystal) at 218 and 219 K obtained upon lowering of the temperature. Pellet spectrum at 300 K is shown for comparison. Absorption band at 860 cm^{-1} is selected for monitoring the hysteresis loop. (b) Hysteresis loop obtained for [Cu(hfac)$_2$ **NN^{Me}**]$_n$ (single crystal). Phase 2 corresponds to the low-temperature (triclinic) geometry, whereas Phase 1 corresponds to the high-temperature (monoclinic) geometry. Arrows indicate the direction of the temperature change.

^{1}H, ^{13}C NMR, IR and Mass Spectra

3,3,4-Trimethyl-1-(1-methyl-1H-pyrazol-4-yl)-4-nitropentan-1-one ***(13a).***

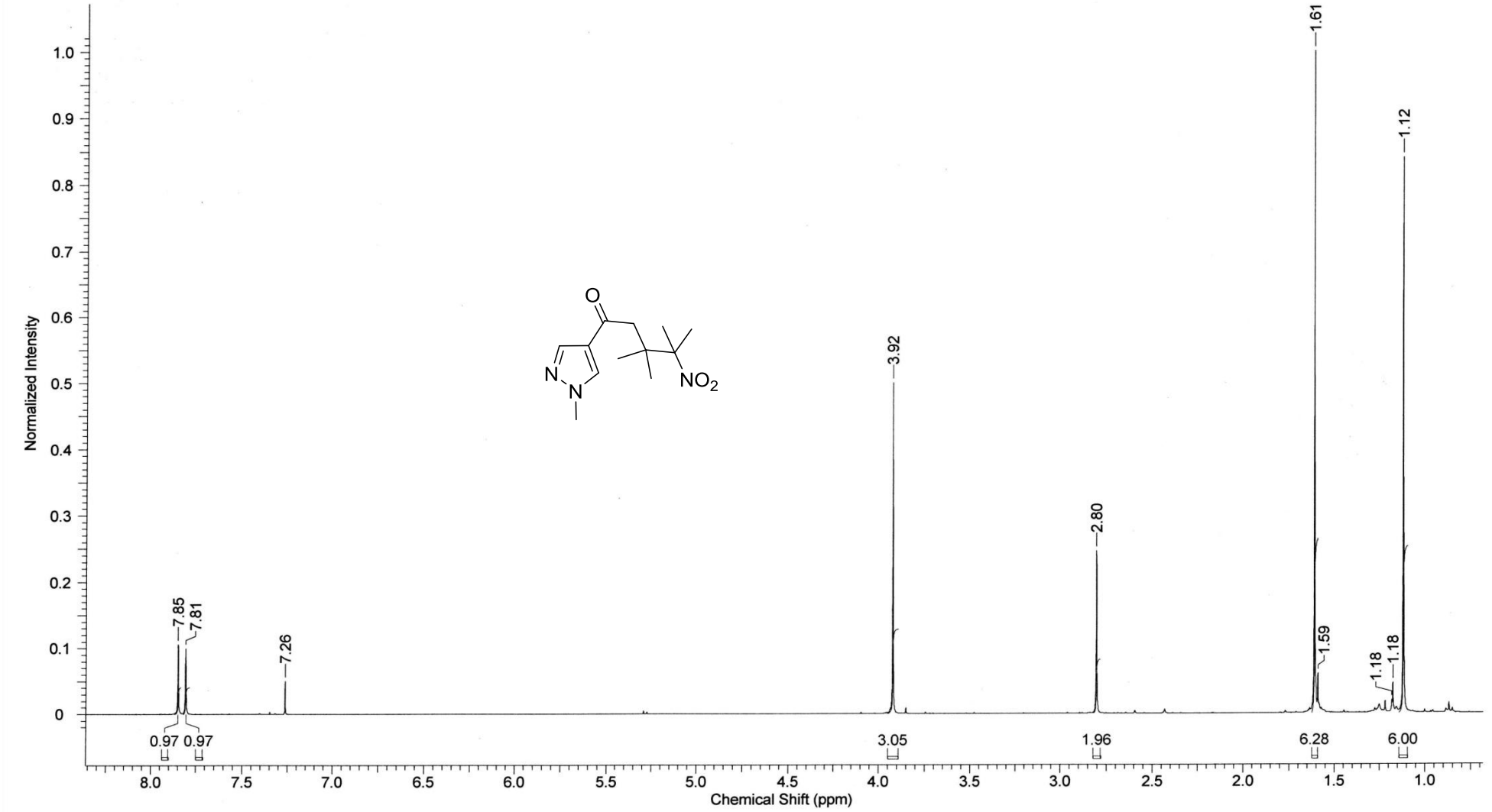

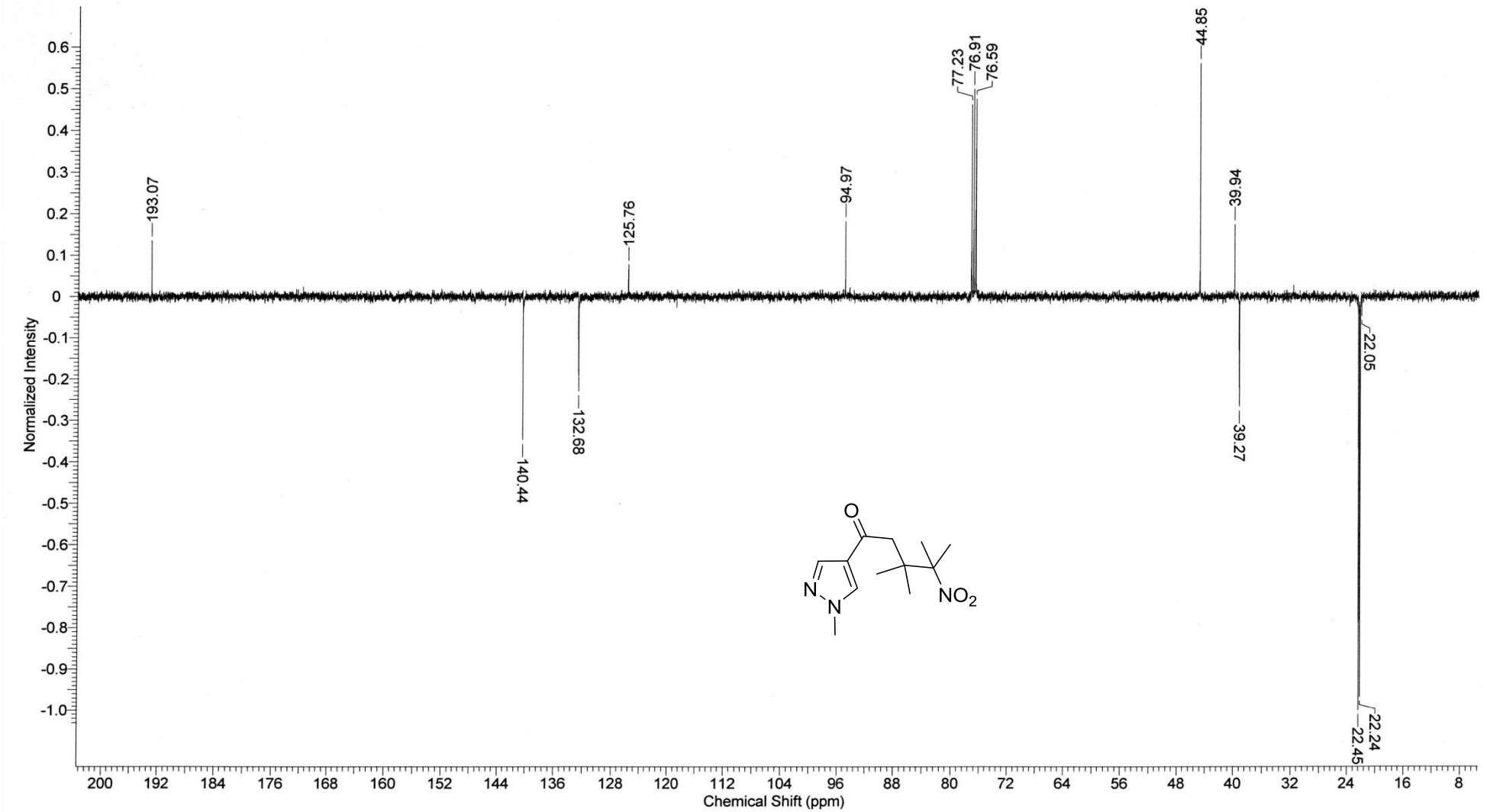
193.07
140.44
132.68
125.76
94.97
77.23
76.91
76.59
44.85
39.94
39.27
22.05
22.24
22.45
Normalized Intensity
Chemical Shift (ppm)
O
N
N
NO2

*3,3,4-Trimethyl-1-(1-ethyl-1H-pyrazol-4-yl)-4-nitropentan-1-one (**13b**)*

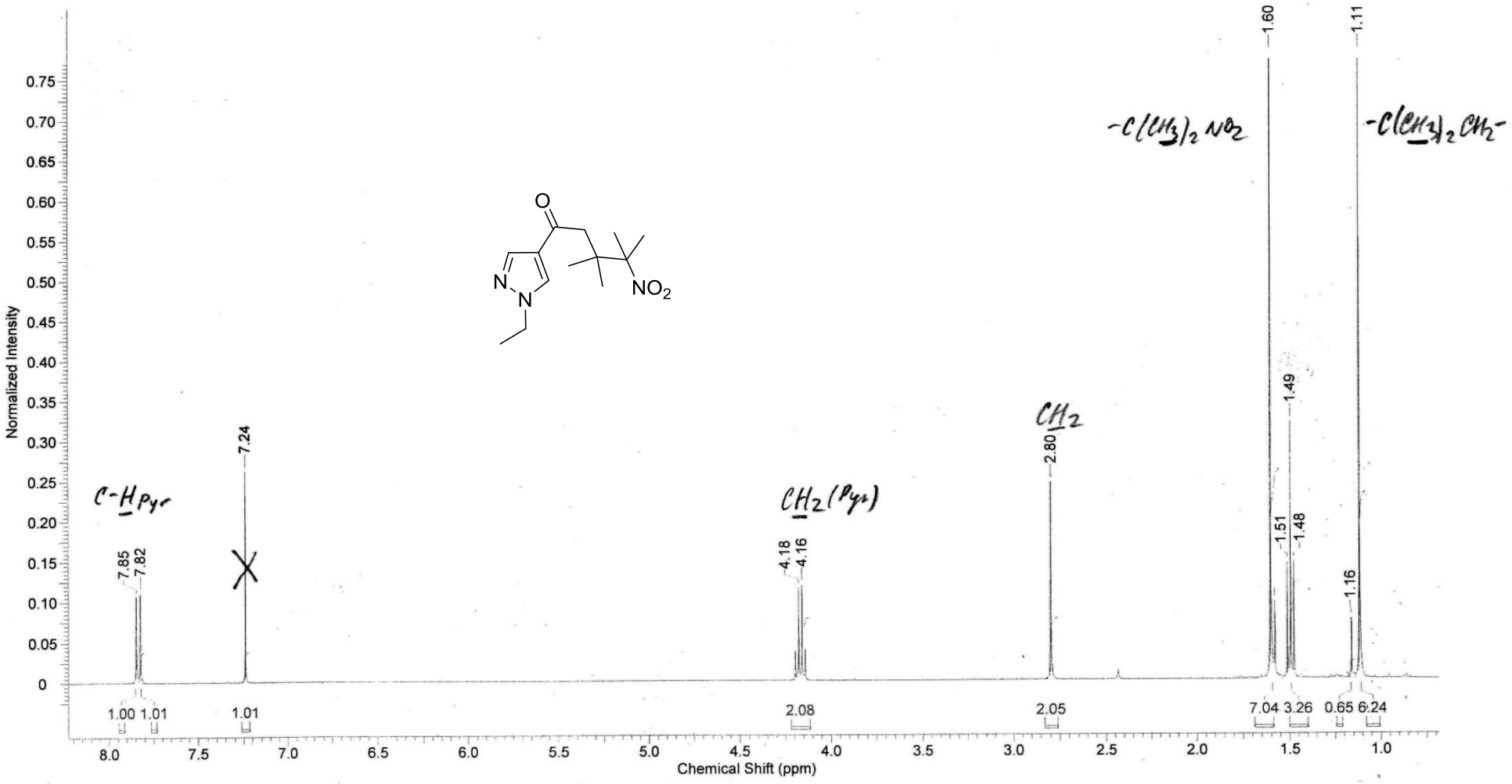

*3,3,4-Trimethyl-1-(1-propyl-1H-pyrazol-4-yl)-4-nitropentan-1-one (**13c**)*

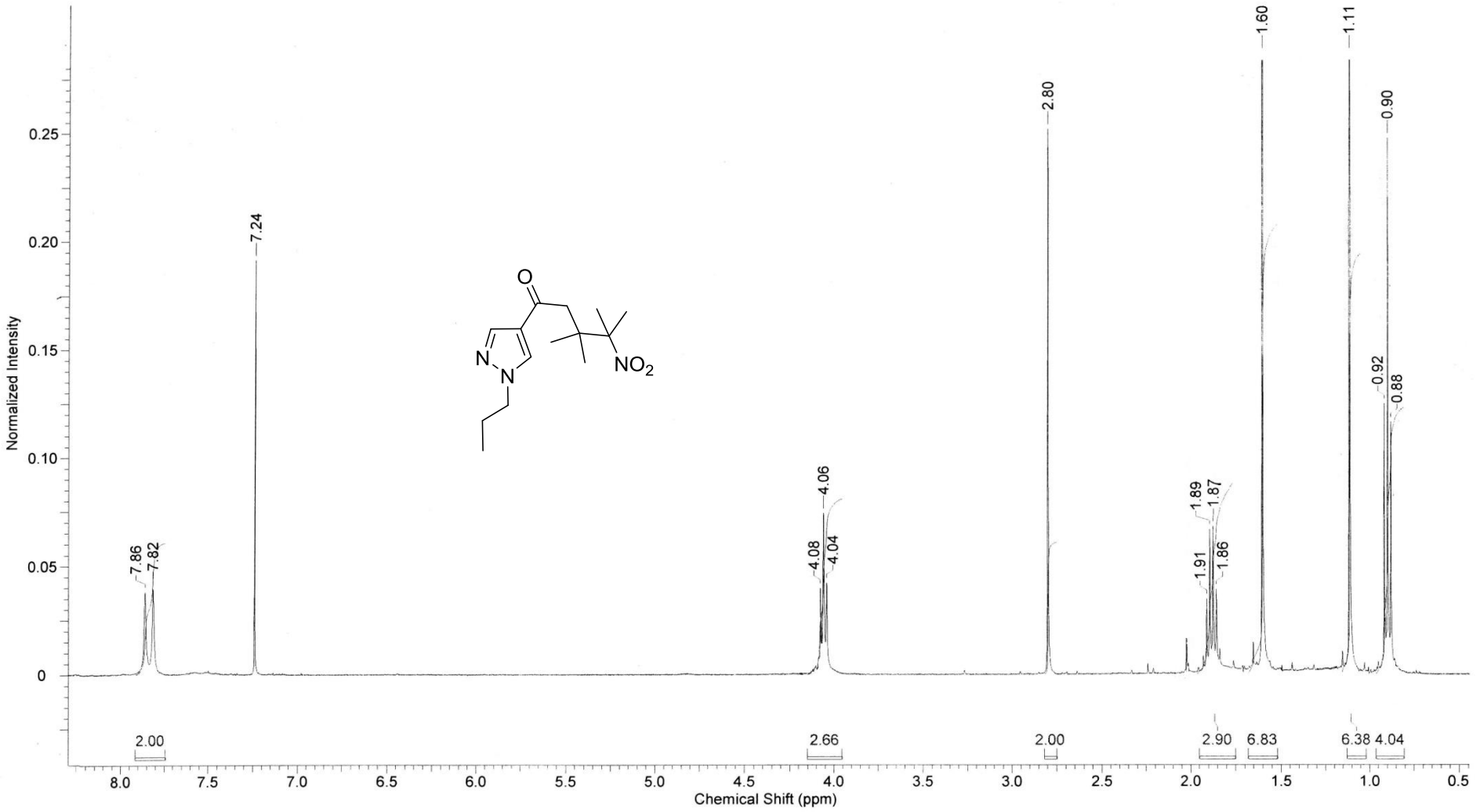

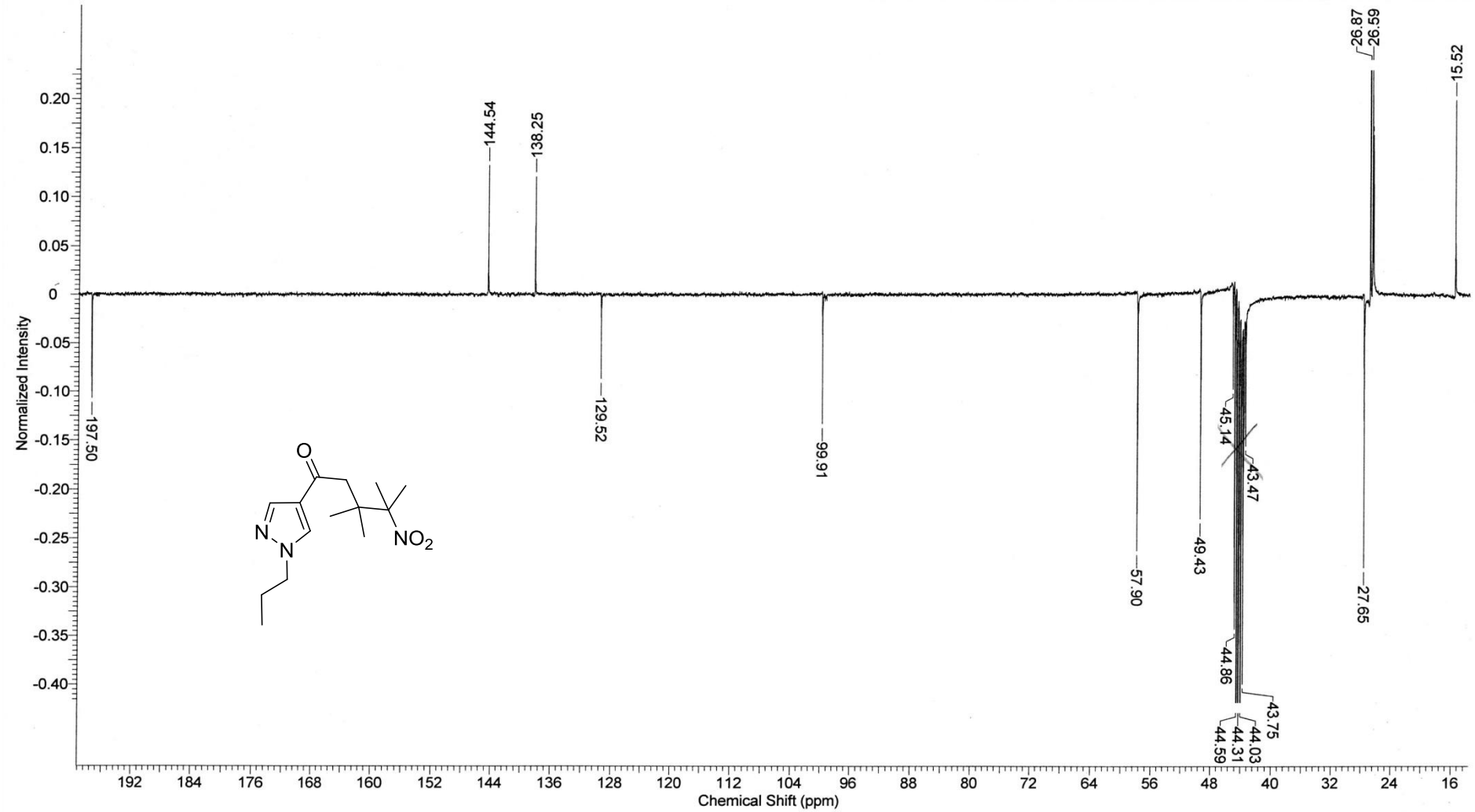
Normalized Intensity
Chemical Shift (ppm)
197.50
144.54
138.25
129.52
99.91
57.90
49.43
45.14
43.47
44.86
43.75
44.03
44.31
44.59
27.65
26.87
26.59
15.52
O
N
N
NO2

*3,3,4-Trimethyl-1-(1-butyl-1H-pyrazol-4-yl)-4-nitropentan-1-one (**13d**)*

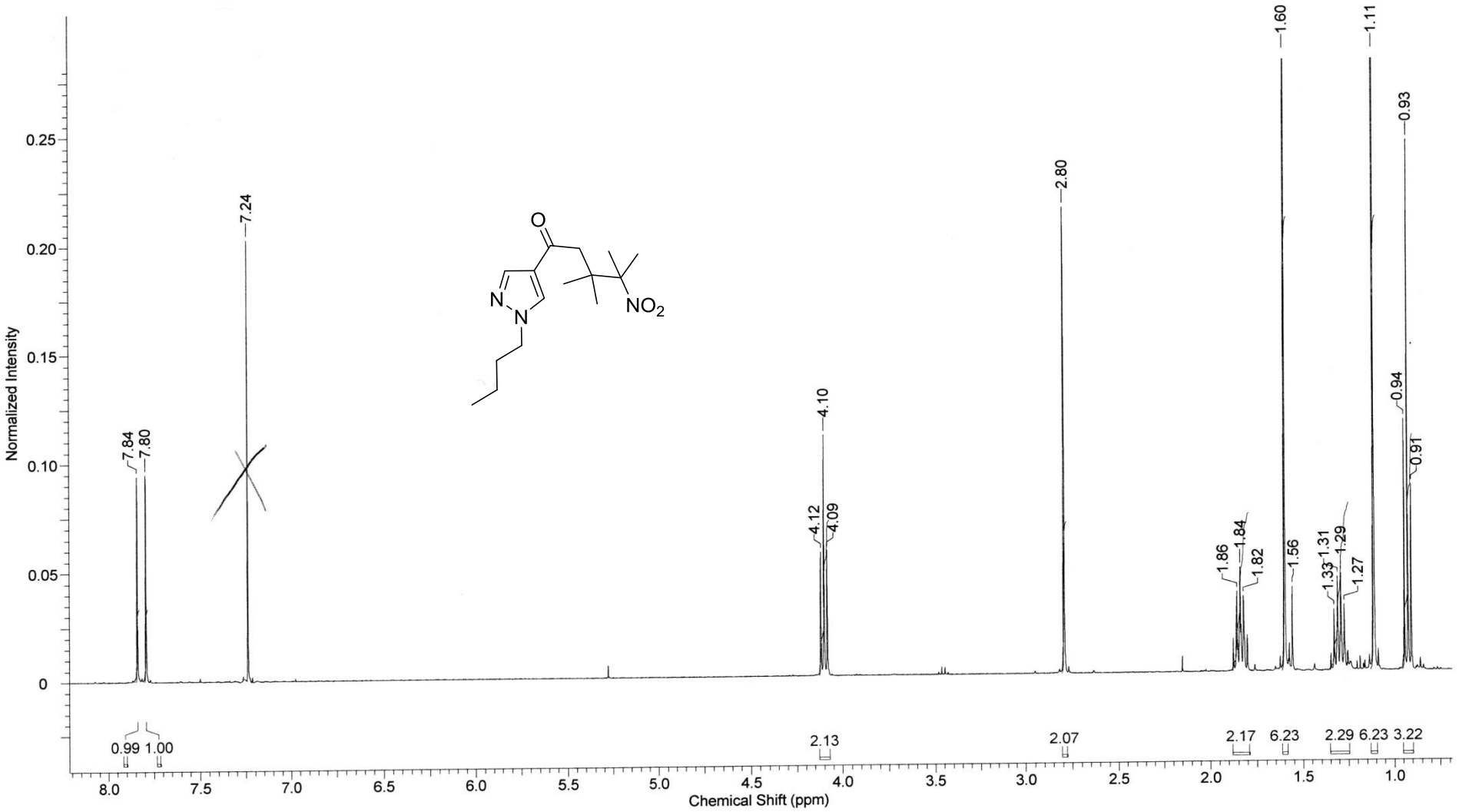

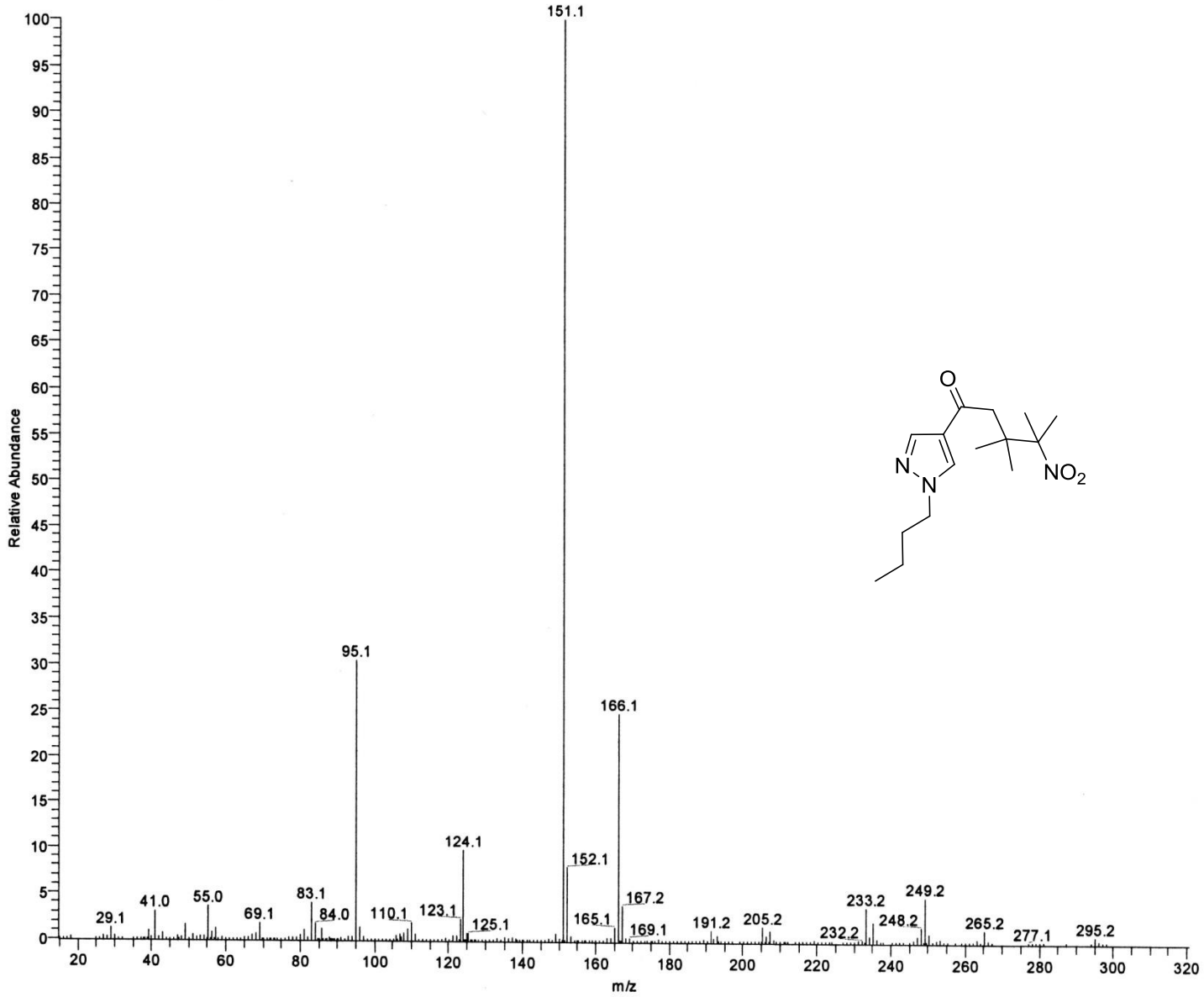
Relative Abundance
m/z
151.1
95.1
166.1
124.1
152.1
167.2
233.2
249.2
41.0
55.0
83.1
29.1
69.1
84.0
110.1
123.1
125.1
165.1
169.1
191.2
205.2
232.2
248.2
265.2
277.1
295.2
O
N
N
NO2

*2,2,3,3-Tetramethyl-5-(1-methyl-1H-pyrazol-4-yl)-3,4-dihydro-2H-pyrrole 1-oxide (**14a**)*

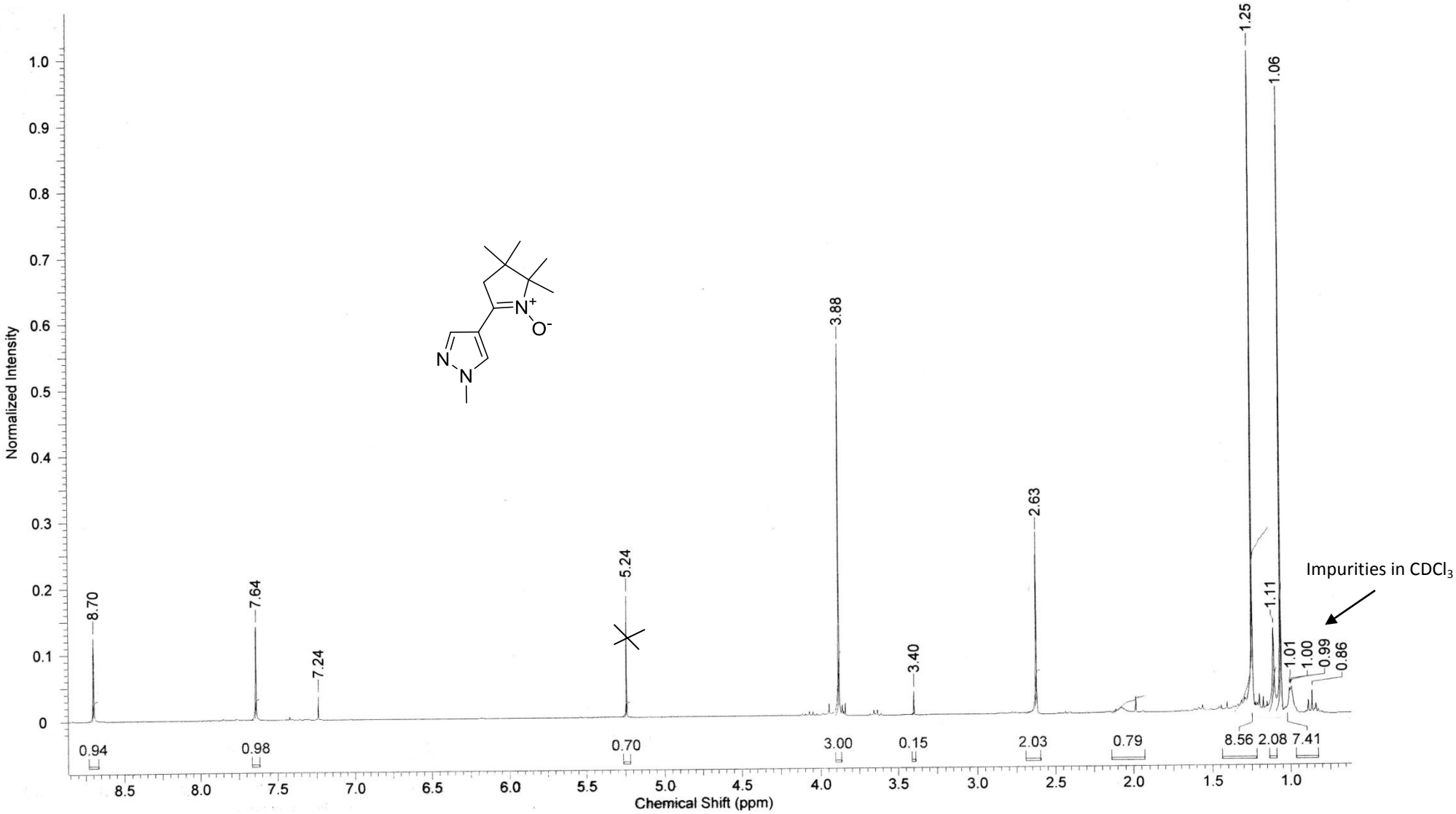

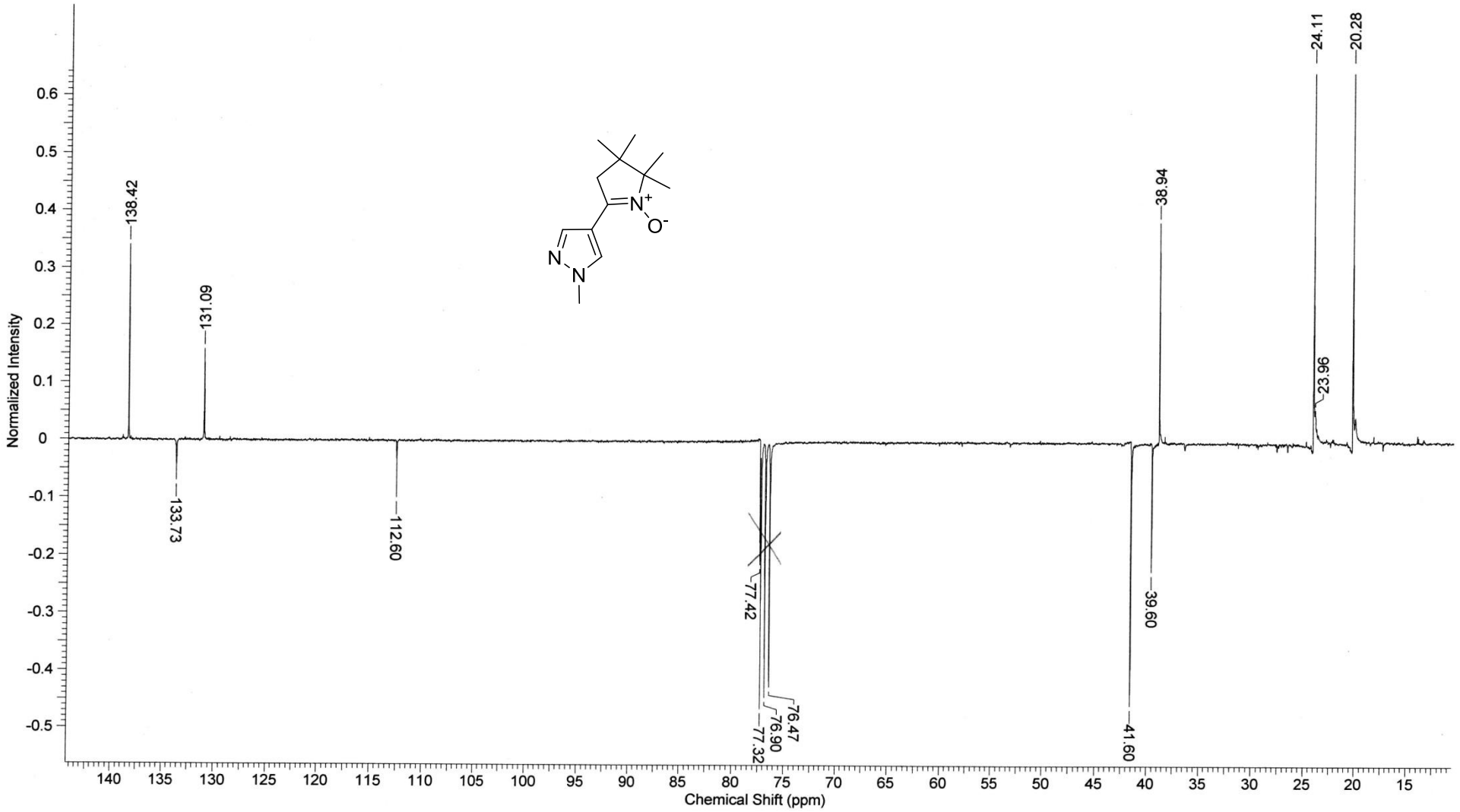
138.42
131.09
133.73
112.60
77.42
77.32
76.90
76.47
38.94
39.60
41.60
24.11
23.96
20.28
Normalized Intensity
Chemical Shift (ppm)

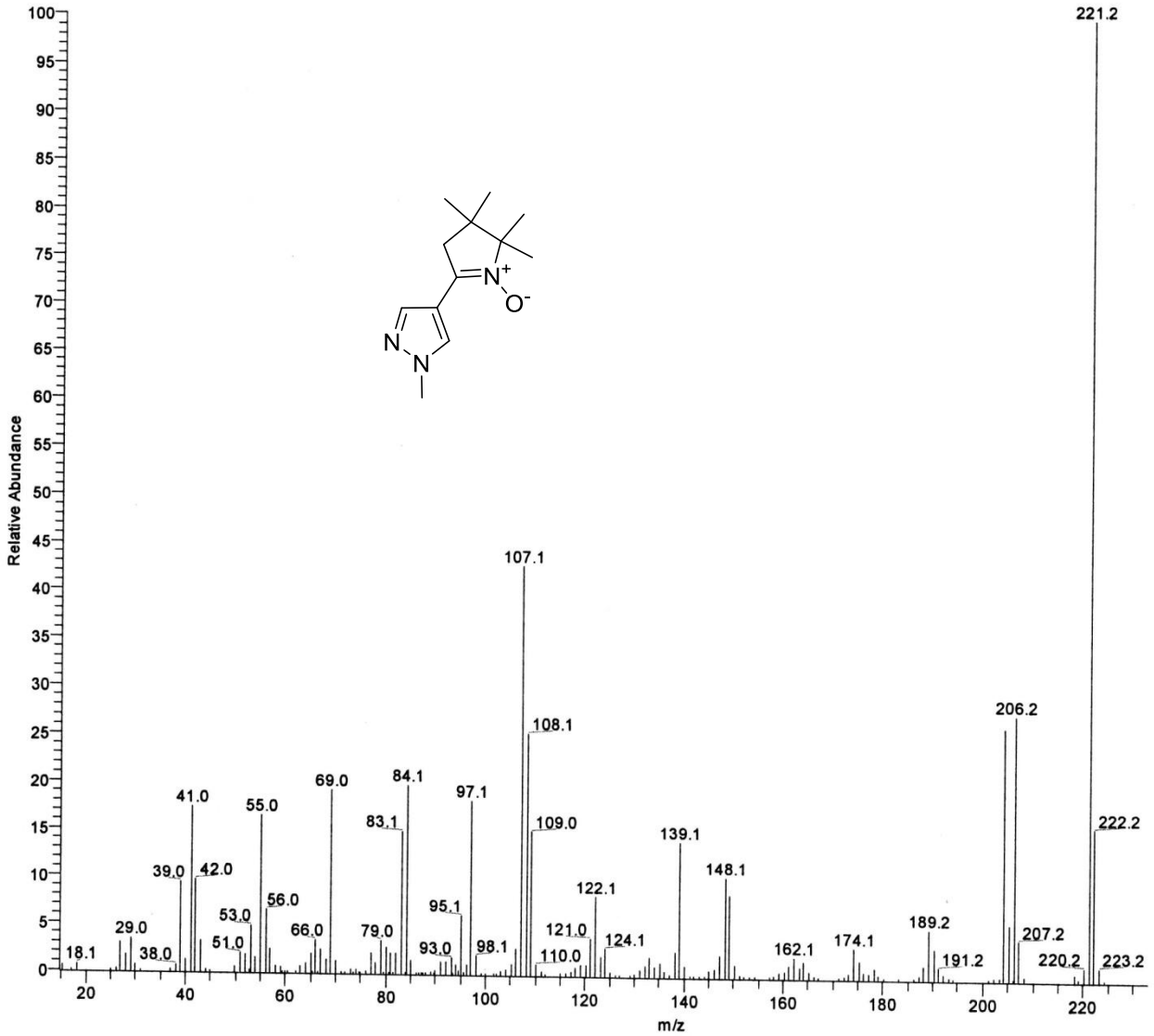
Relative Abundance
m/z
221.2
107.1
108.1
206.2
84.1
69.0
97.1
41.0
55.0
109.0
222.2
83.1
139.1
148.1
39.0
42.0
122.1
56.0
95.1
53.0
29.0
66.0
79.0
121.0
189.2
207.2
18.1
38.0
51.0
93.0
98.1
110.0
124.1
162.1
174.1
191.2
220.2
223.2

*2,2,3,3-Tetramethyl-5-(1-ethyl-1H-pyrazol-4-yl)-3,4-dihydro-2H-pyrrole 1-oxide (**14b**)*

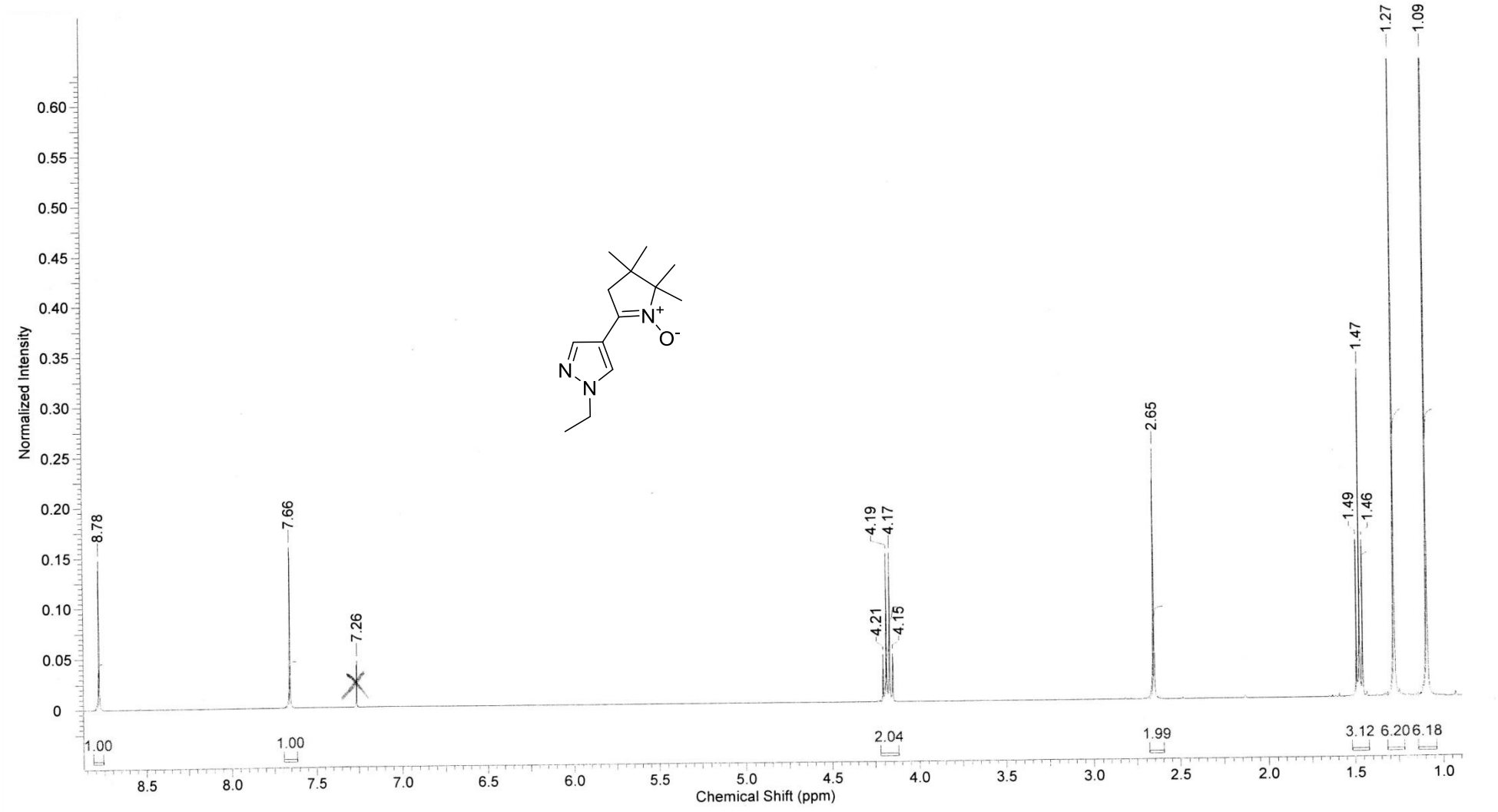

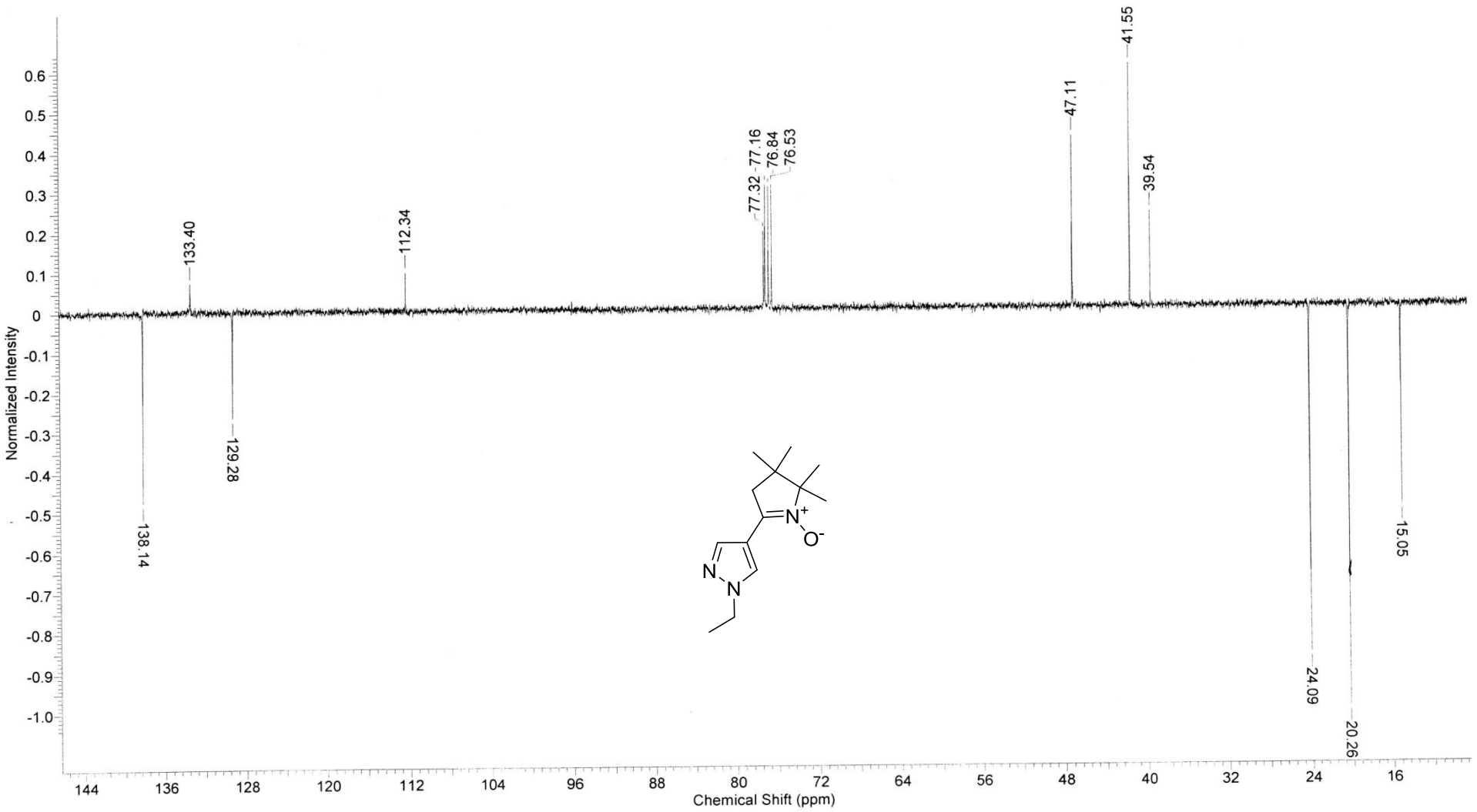
Normalized Intensity
Chemical Shift (ppm)
133.40
112.34
77.32
77.16
76.84
76.53
47.11
41.55
39.54
138.14
129.28
24.09
20.26
15.05
N+
O-
N
N

*2,2,3,3-Tetramethyl-5-(1-propyl-1H-pyrazol-4-yl)-3,4-dihydro-2H-pyrrole 1-oxide (**14c**)*

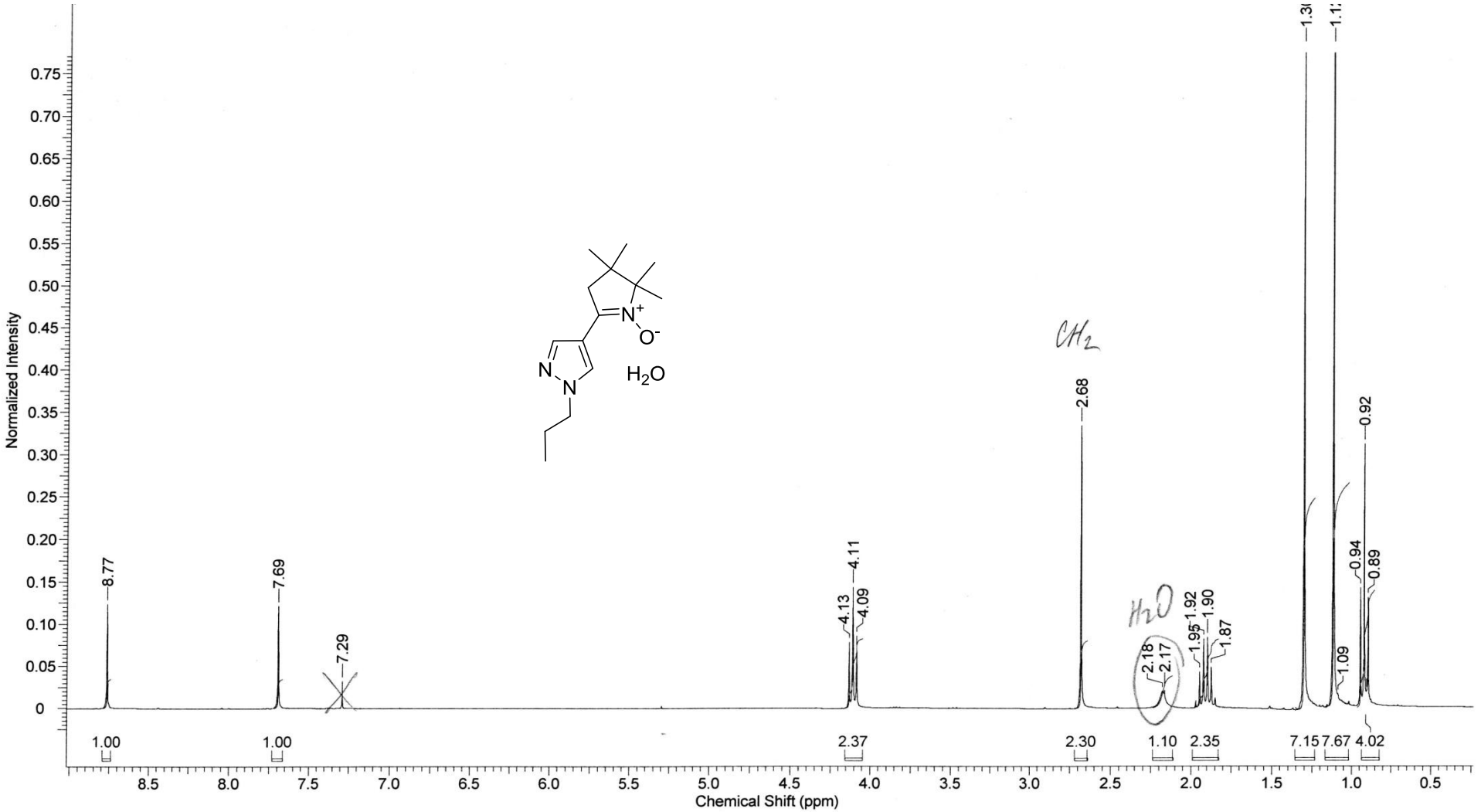

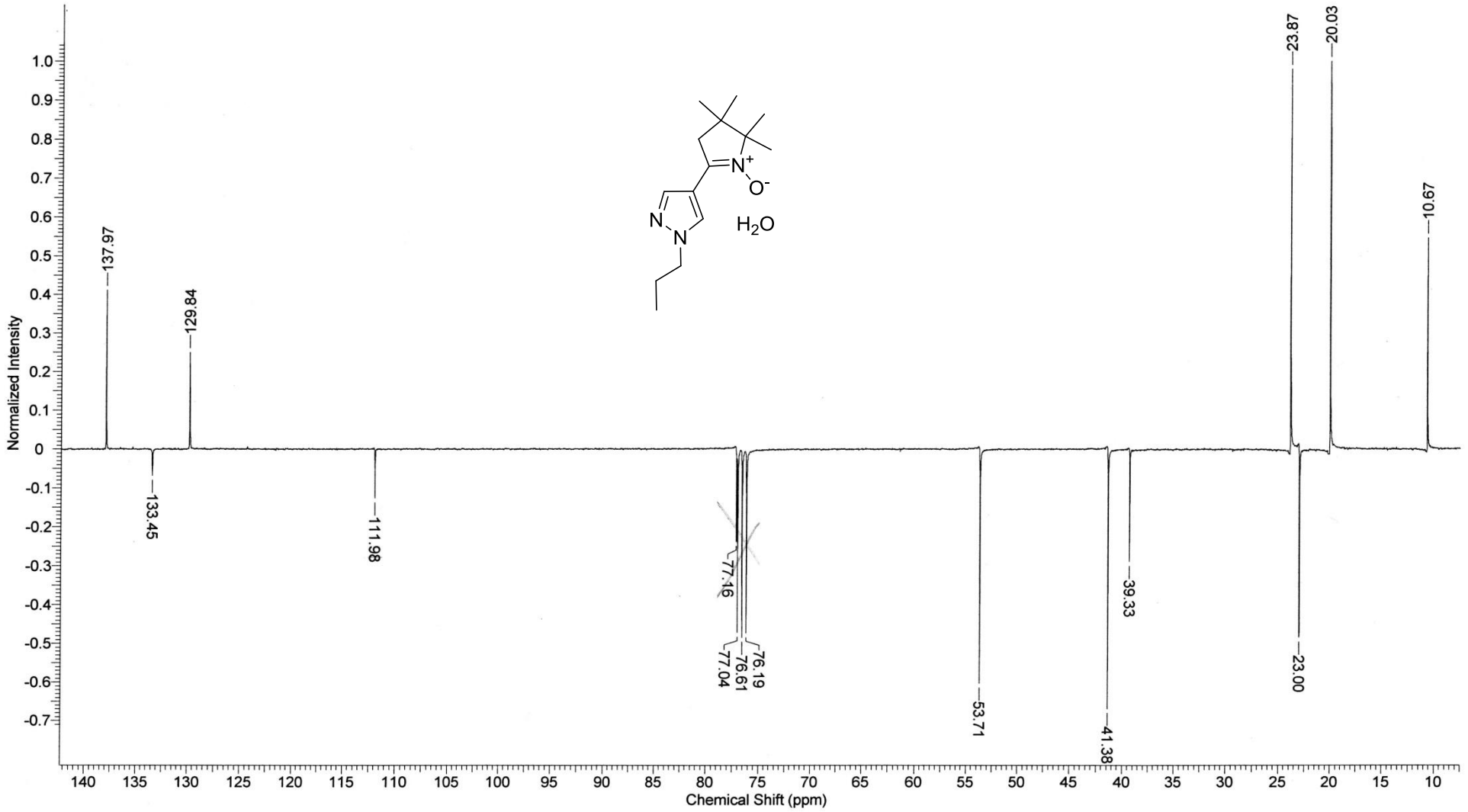
137.97
129.84
133.45
111.98
77.16
77.04
76.61
76.19
53.71
41.38
39.33
23.87
23.00
20.03
10.67
Normalized Intensity
Chemical Shift (ppm)
H2O

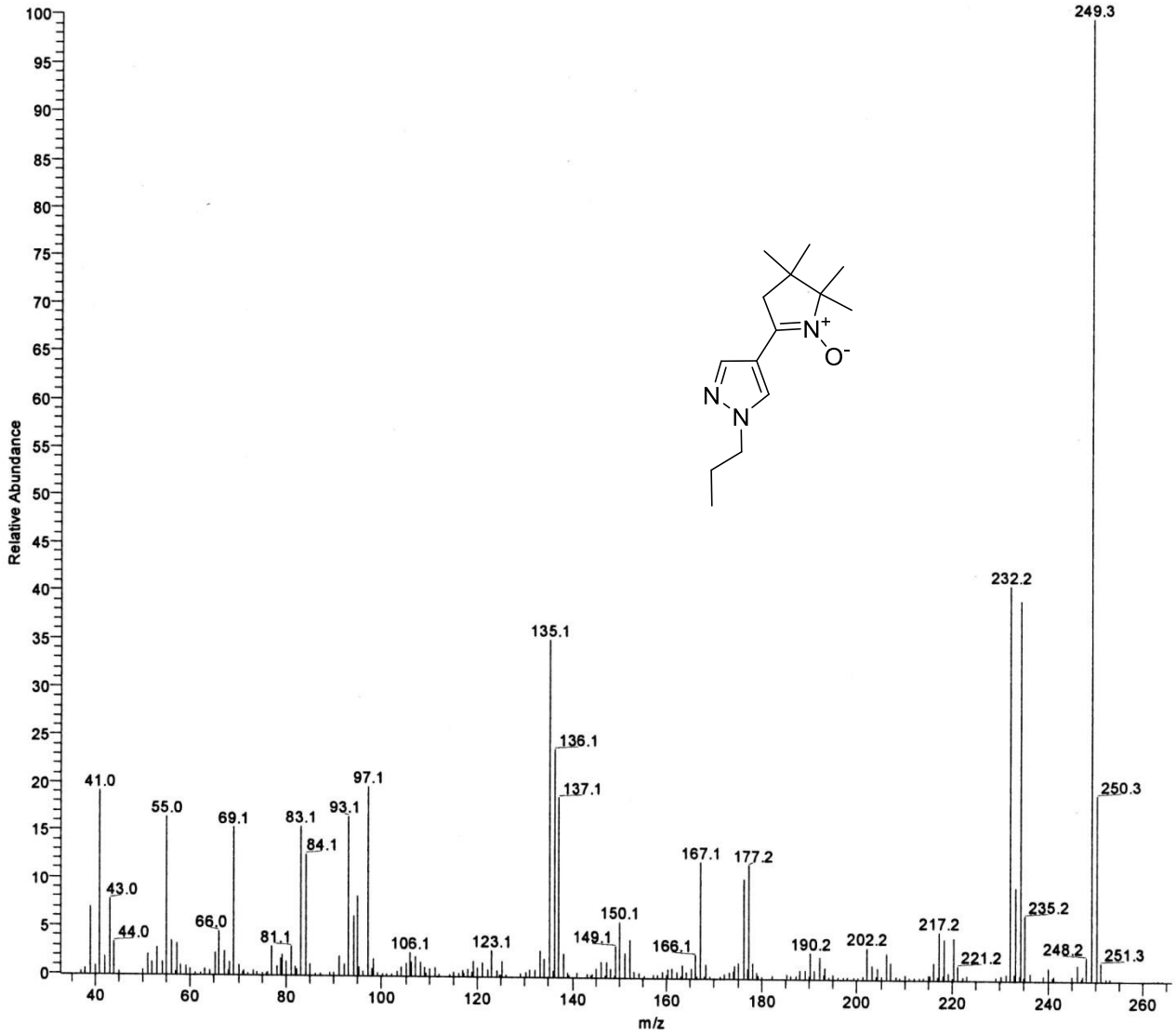
Relative Abundance
m/z
249.3
232.2
135.1
136.1
137.1
250.3
97.1
41.0
55.0
69.1
83.1
93.1
84.1
167.1
177.2
43.0
150.1
235.2
66.0
44.0
81.1
106.1
123.1
149.1
166.1
190.2
202.2
217.2
221.2
248.2
251.3
N+
O-
N
N

2,2,3,3-Tetramethyl-5-(1-butyl-1H-pyrazol-4-yl)-3,4-dihydro-2H-pyrrole 1-oxide ***(14d)***

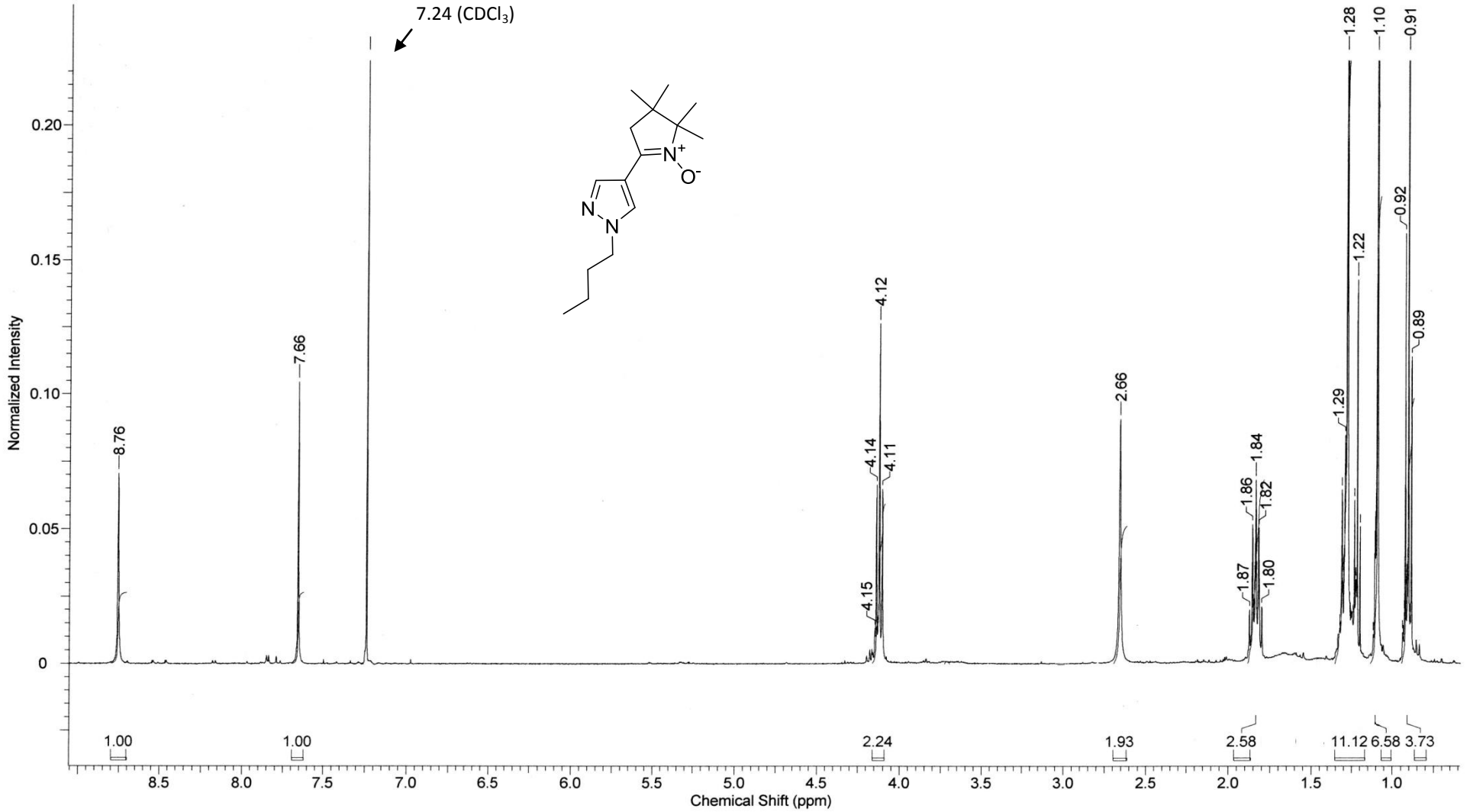

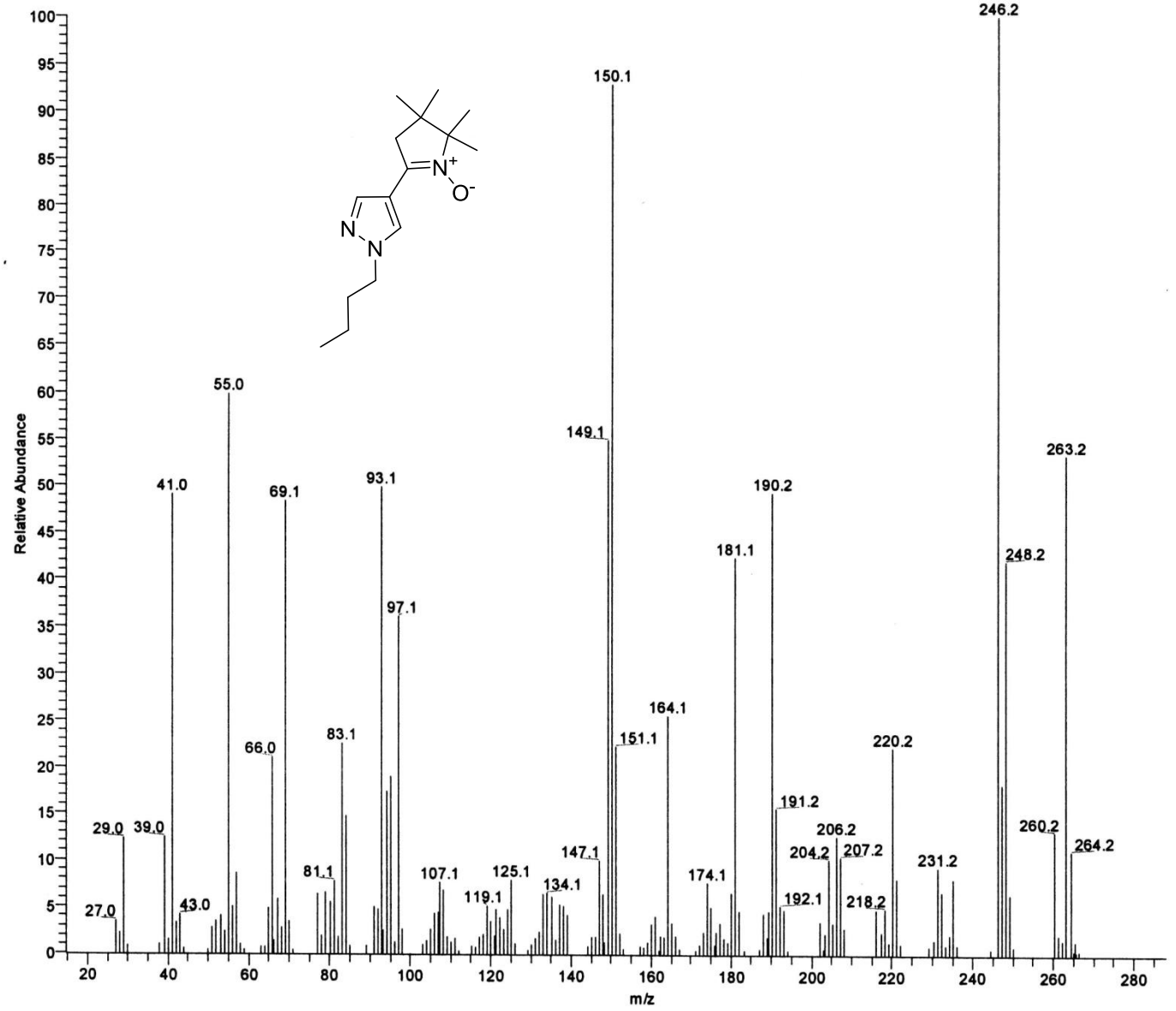
Relative Abundance
m/z
246.2
150.1
149.1
263.2
55.0
41.0
69.1
93.1
190.2
181.1
248.2
97.1
164.1
151.1
83.1
66.0
220.2
191.2
206.2
260.2
264.2
204.2
207.2
231.2
147.1
174.1
81.1
107.1
125.1
134.1
119.1
192.1
218.2
29.0
39.0
43.0
27.0

*2,2,3,3-Tetramethyl-5-(1-methyl-1H-pyrazol-4-yl)-4-oxo-3,4-dihydro-2H-pyrrole 1-oxide (**4a**)*

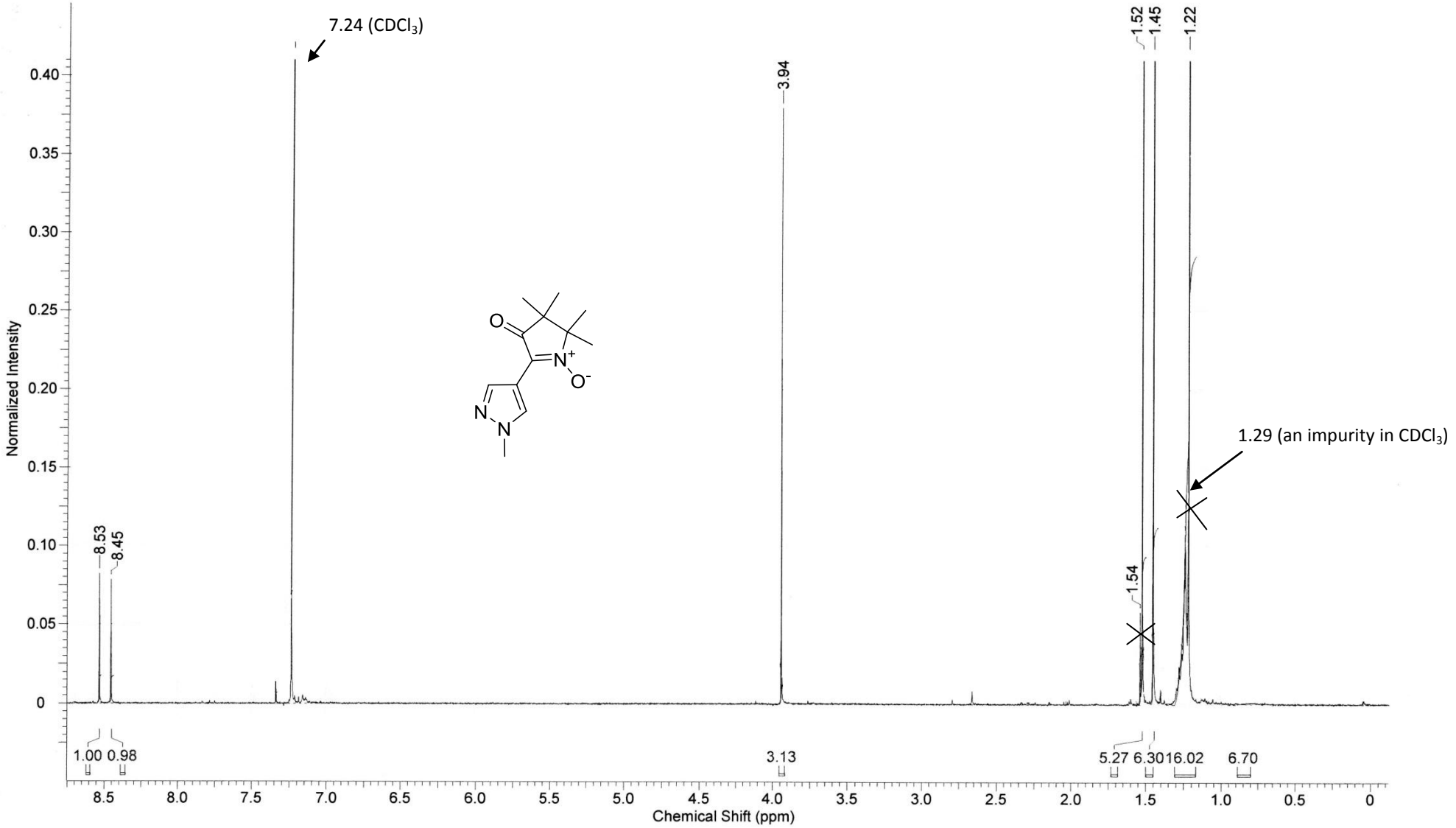

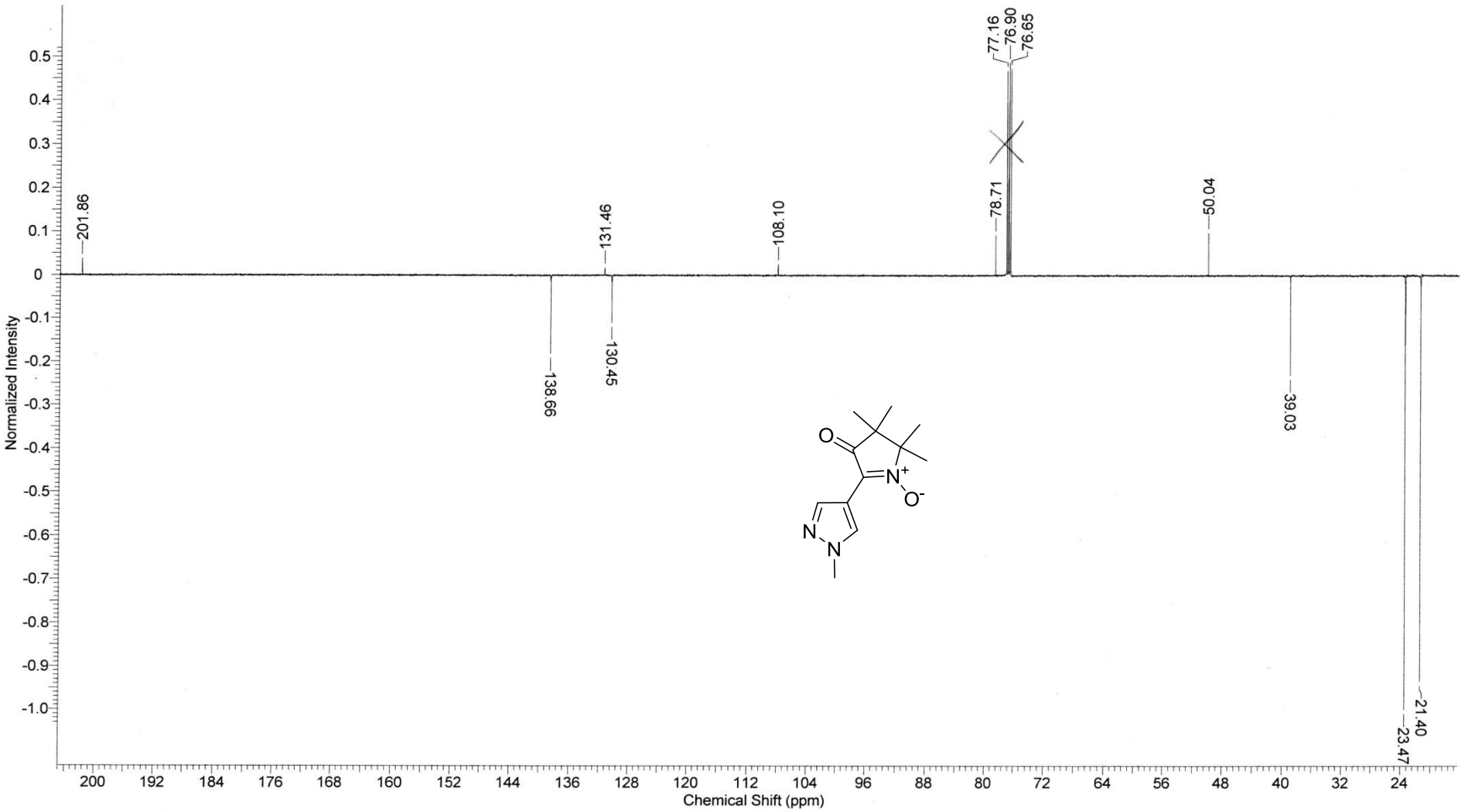
201.86
138.66
131.49
130.45
108.10
77.16
76.90
76.65
78.71
50.04
39.03
23.47
21.40
Normalized Intensity
Chemical Shift (ppm)
O
N+
O-
N
N

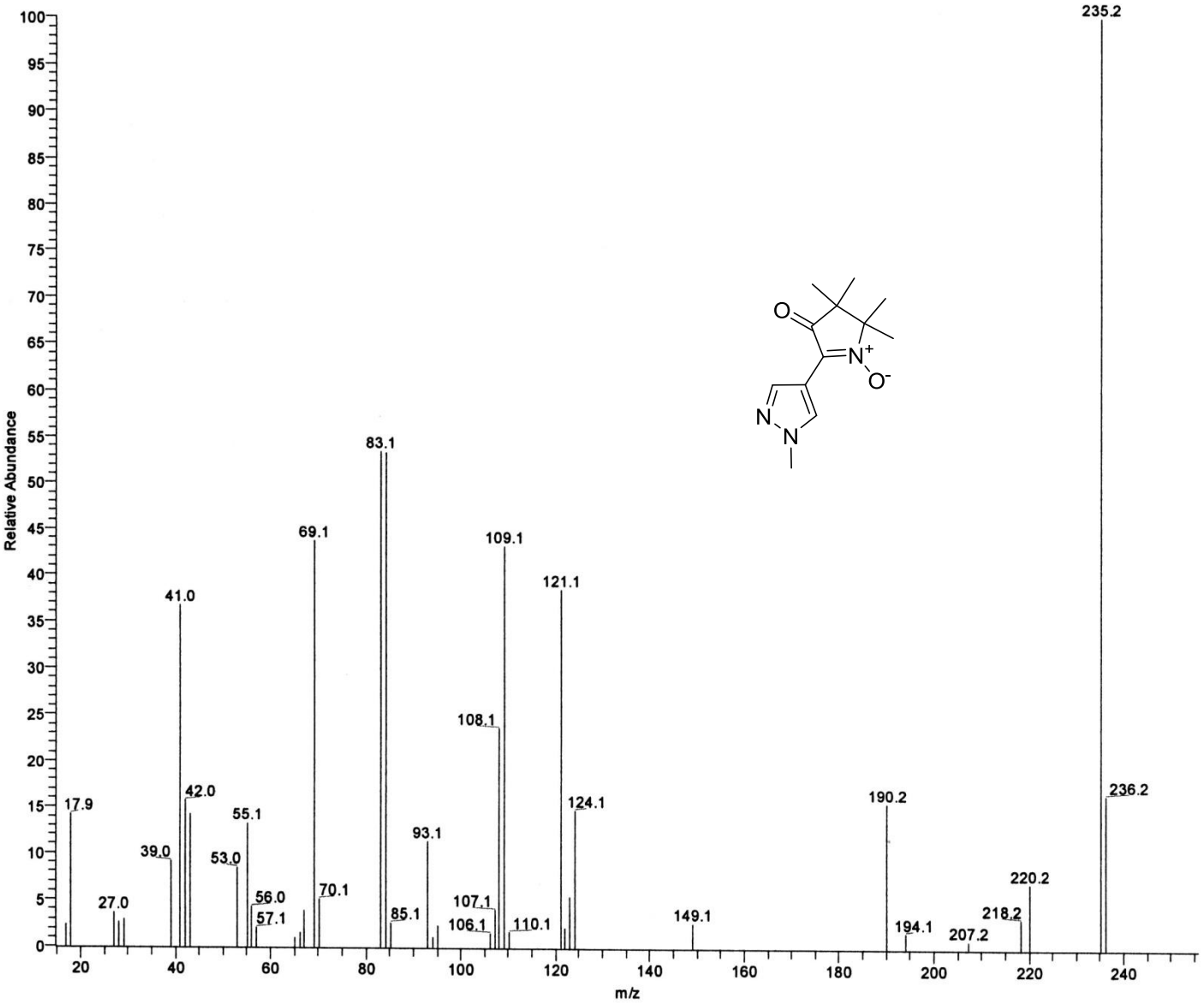
Relative Abundance
m/z
235.2
83.1
69.1
109.1
121.1
41.0
108.1
42.0
124.1
236.2
190.2
17.9
55.1
93.1
39.0
53.0
220.2
70.1
56.0
27.0
107.1
85.1
218.2
57.1
106.1
110.1
149.1
194.1
207.2
O
N+
O-
N
N

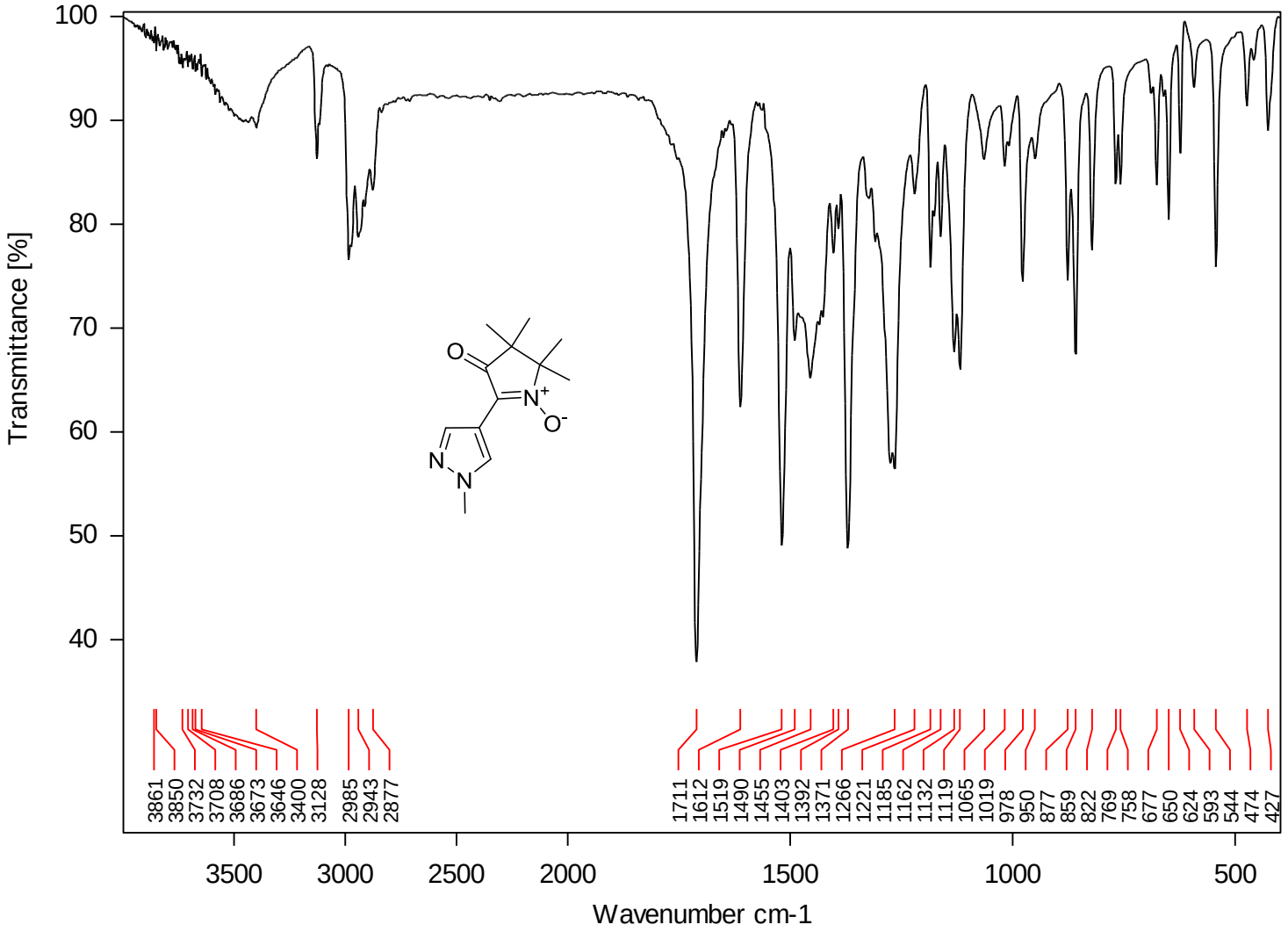
Transmittance [%]
100
90
80
70
60
50
40
3861
3850
3732
3708
3686
3673
3646
3400
3128
2985
2943
2877
1711
1612
1519
1490
1455
1403
1392
1371
1266
1221
1185
1162
1132
1119
1065
1019
978
950
877
859
822
769
758
677
650
624
593
544
474
427
3500
3000
2500
2000
1500
1000
500
Wavenumber cm-1
O
N+
O-
N
N

*2,2,3,3-Tetramethyl-5-(1-ethyl-1H-pyrazol-4-yl)-4-oxo-3,4-dihydro-2H-pyrrole 1-oxide (**4b**)*

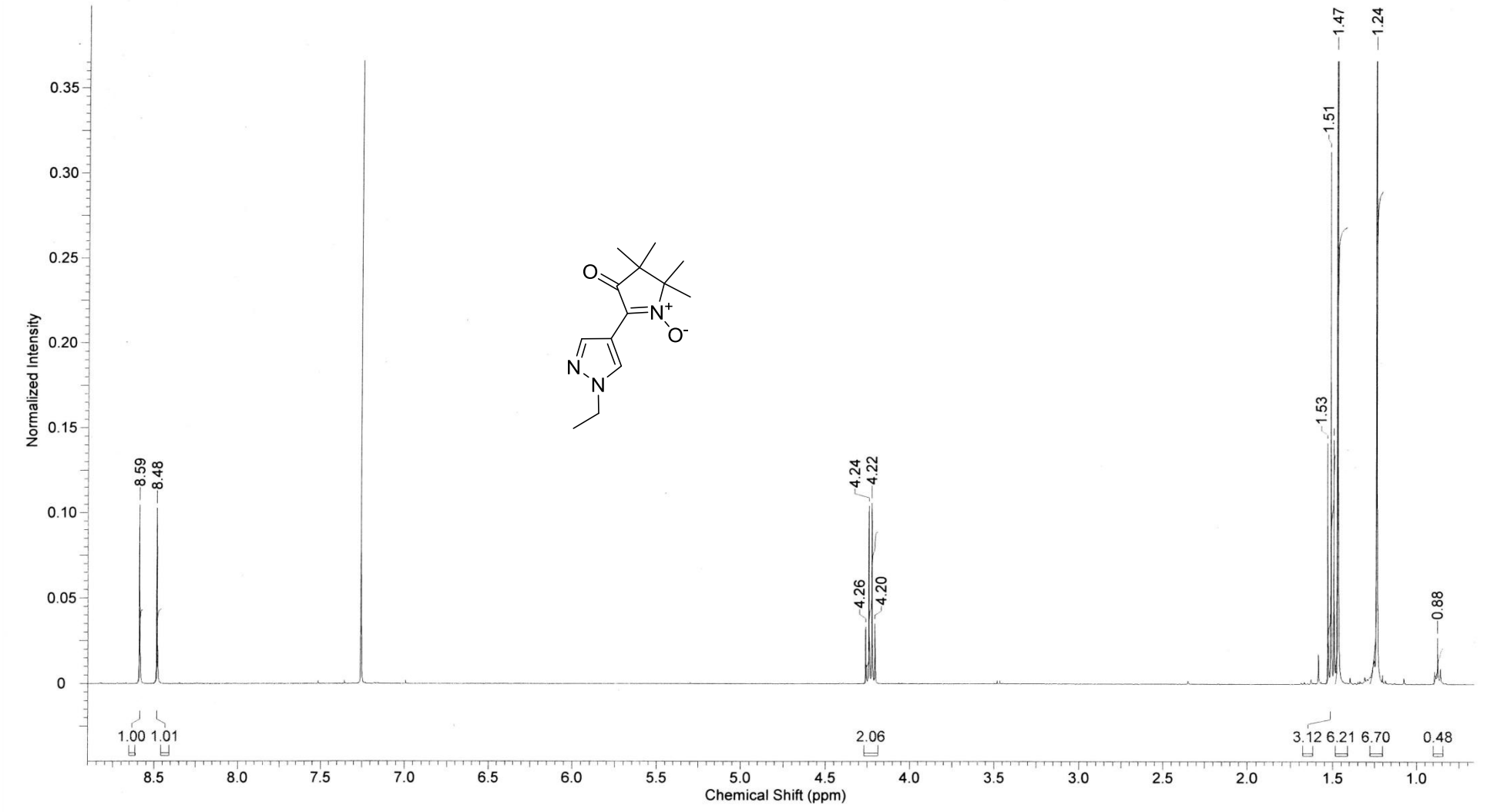

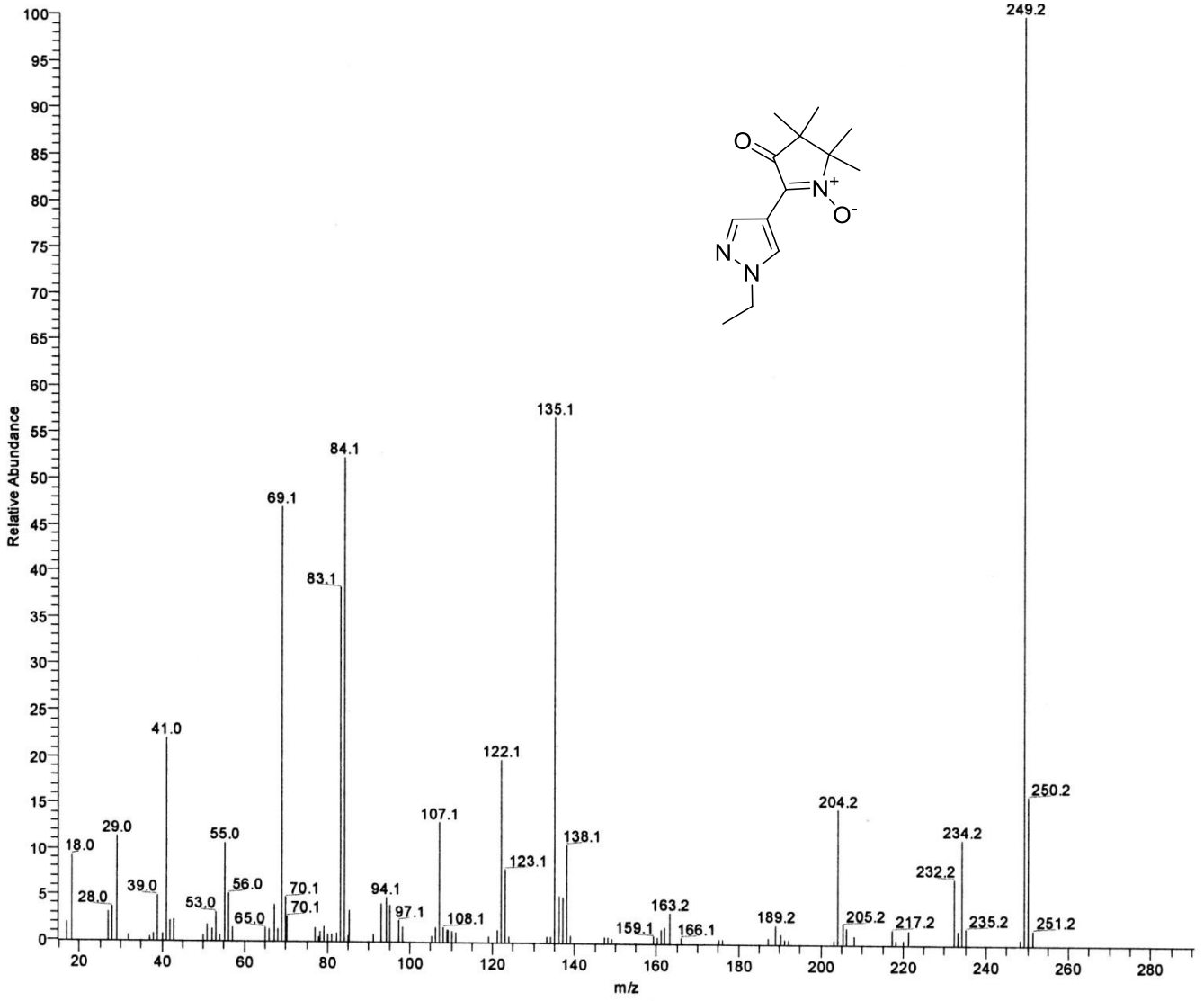
Relative Abundance
m/z
249.2
135.1
84.1
69.1
83.1
41.0
122.1
107.1
138.1
123.1
204.2
250.2
234.2
232.2
55.0
29.0
18.0
56.0
70.1
94.1
39.0
28.0
53.0
65.0
97.1
108.1
163.2
159.1
166.1
189.2
205.2
217.2
235.2
251.2
O
N+
O-
N
N

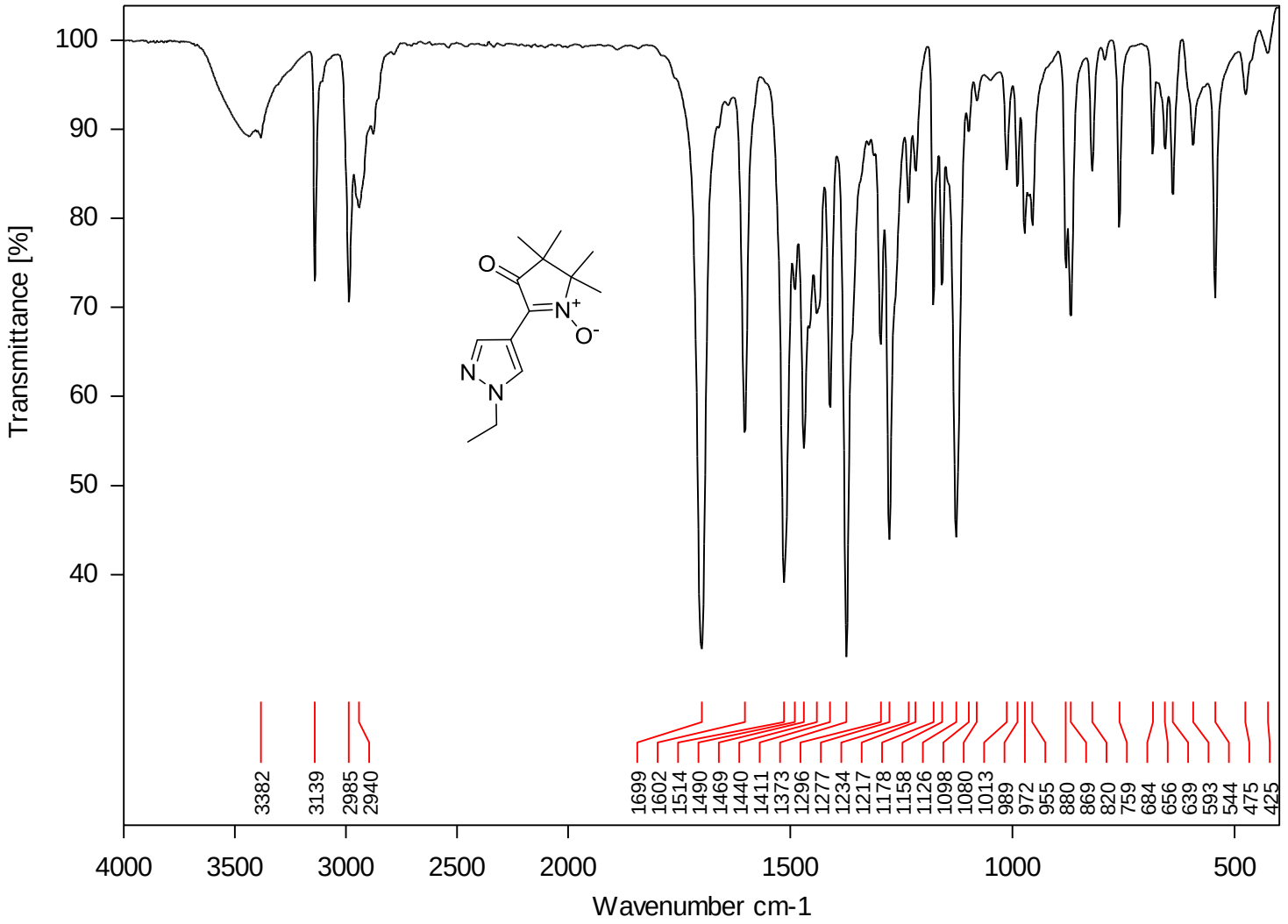
Transmittance [%]
100
90
80
70
60
50
40
O
N+
O-
N
N
3382
3139
2985
2940
1699
1602
1514
1490
1469
1440
1411
1373
1296
1277
1234
1217
1178
1158
1126
1098
1080
1013
989
972
955
880
869
820
759
684
656
639
593
544
475
425
4000
3500
3000
2500
2000
1500
1000
500
Wavenumber cm-1

*2,2,3,3-Tetramethyl-5-(1-propyl-1H-pyrazol-4-yl)-4-oxo-3,4-dihydro-2H-pyrrole 1-oxide (**4c**)*

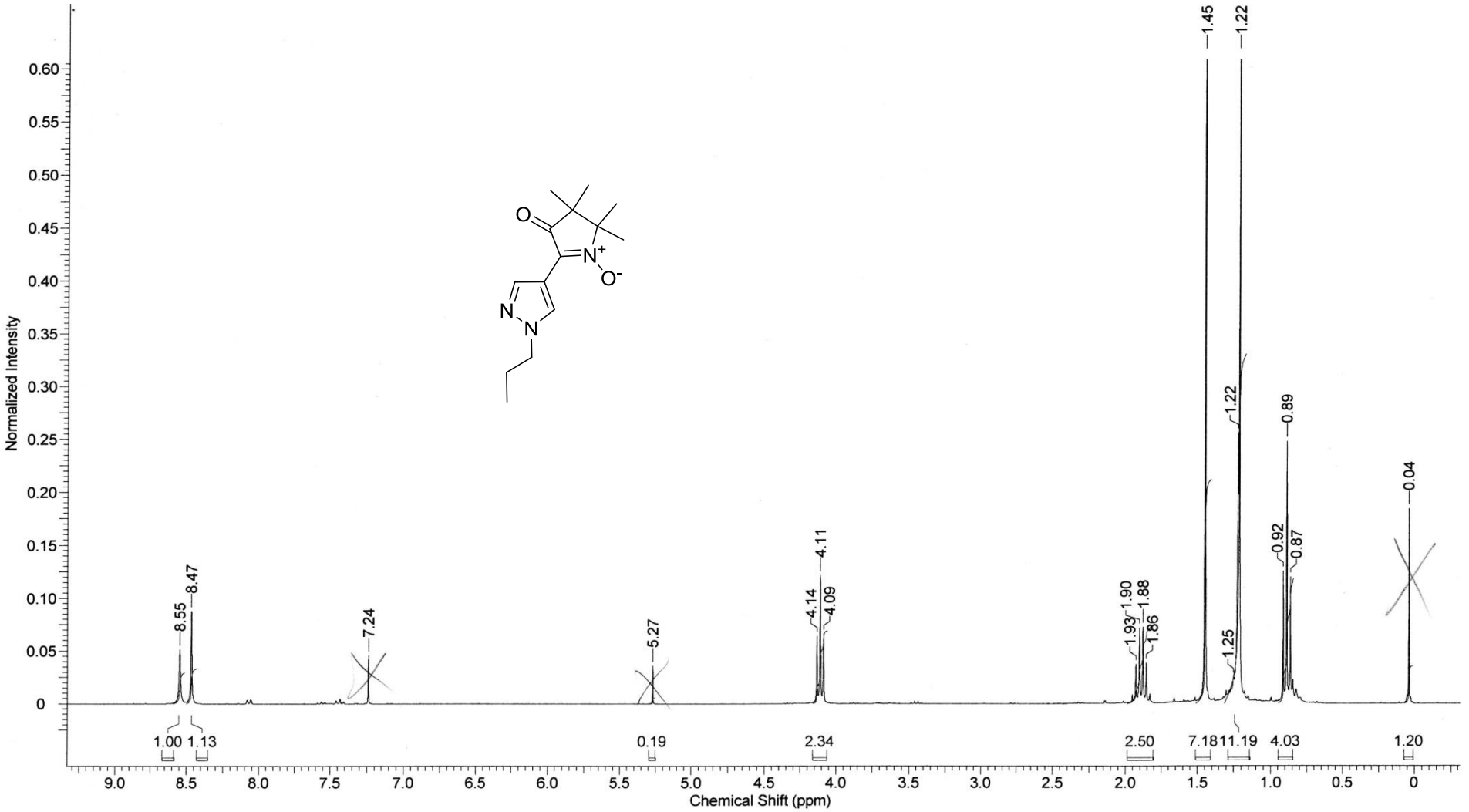

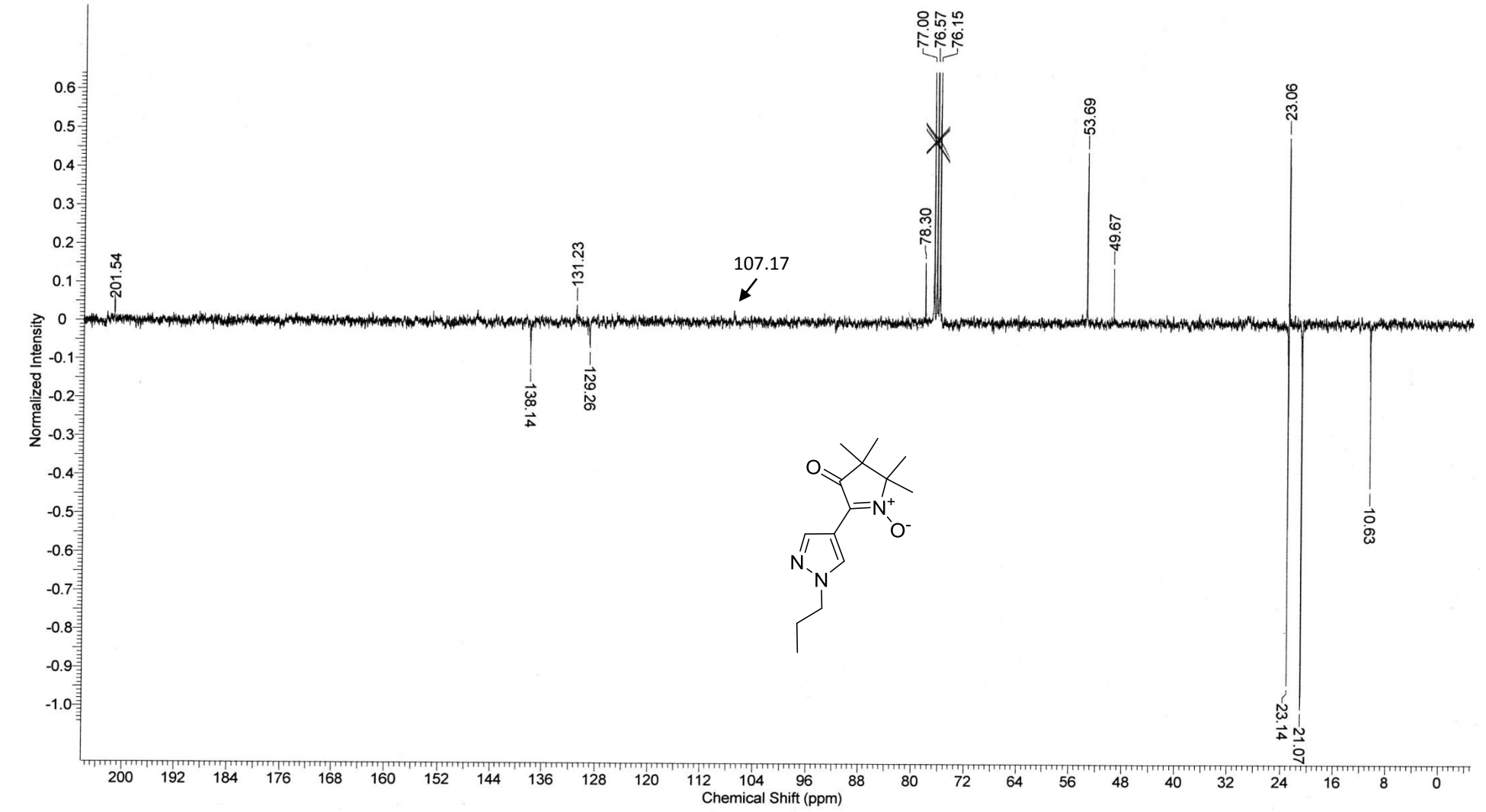
77.00
76.57
76.15
53.69
23.06
78.30
49.67
201.54
131.23
107.17
138.14
129.26
10.63
23.14
21.07
Normalized Intensity
Chemical Shift (ppm)
O
N+
O-
N
N

*2,2,3,3-Tetramethyl-5-(1-butyl-1H-pyrazol-4-yl)-4-oxo-3,4-dihydro-2H-pyrrole 1-oxide (**4d**)*

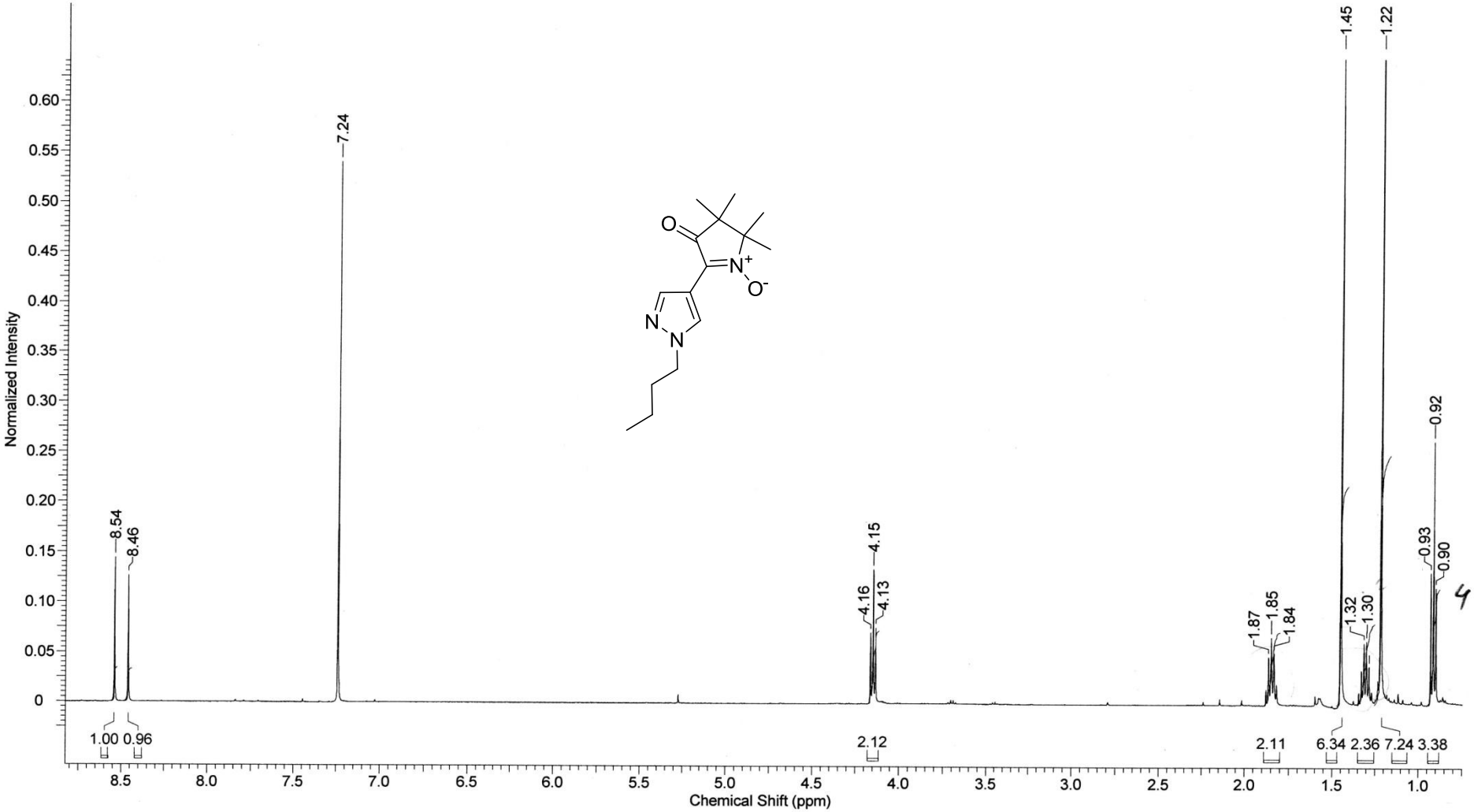

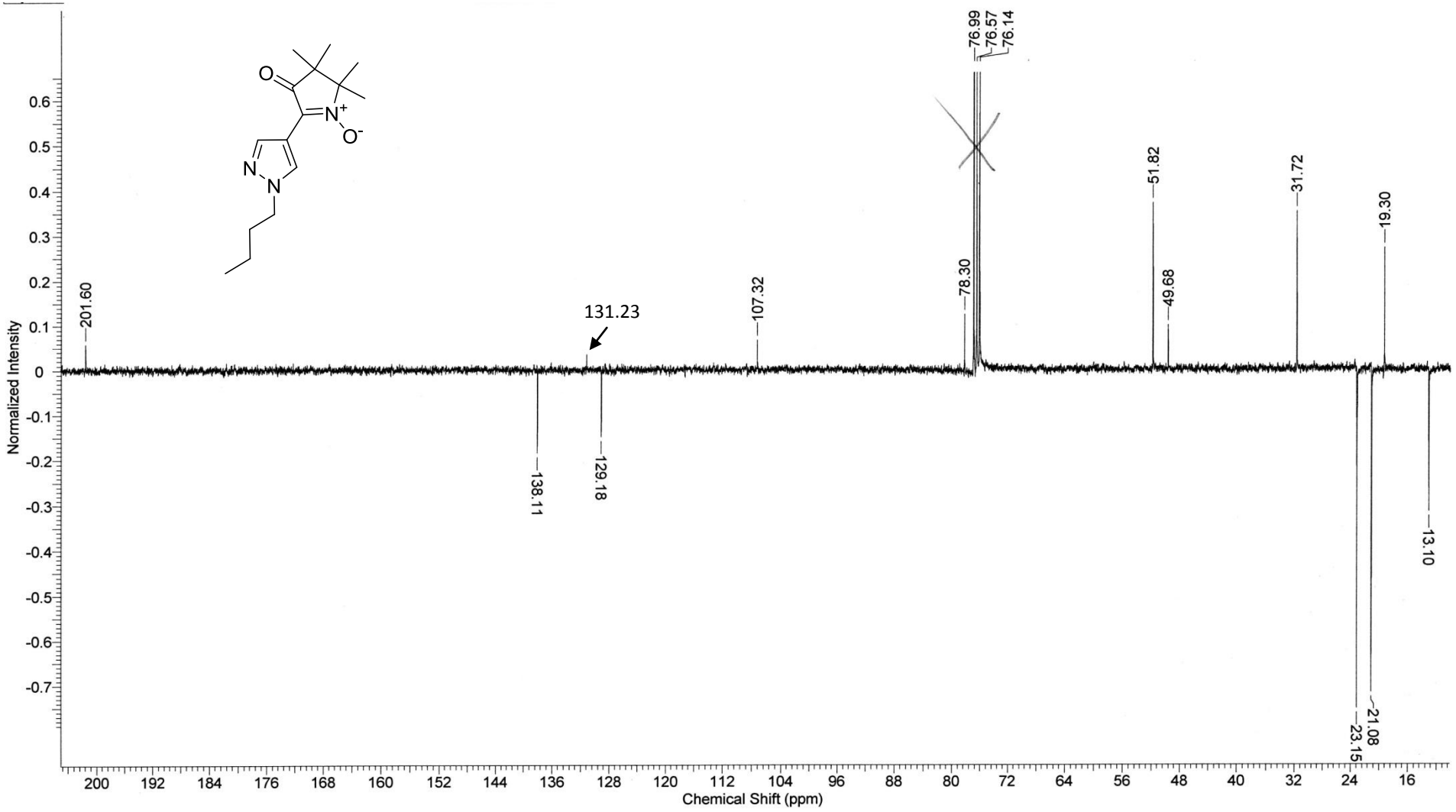
O
N+
O-
N
N
201.60
131.23
107.32
78.30
76.99
76.57
76.14
51.82
49.68
31.72
19.30
138.11
129.18
23.15
21.08
13.10
Normalized Intensity
Chemical Shift (ppm)

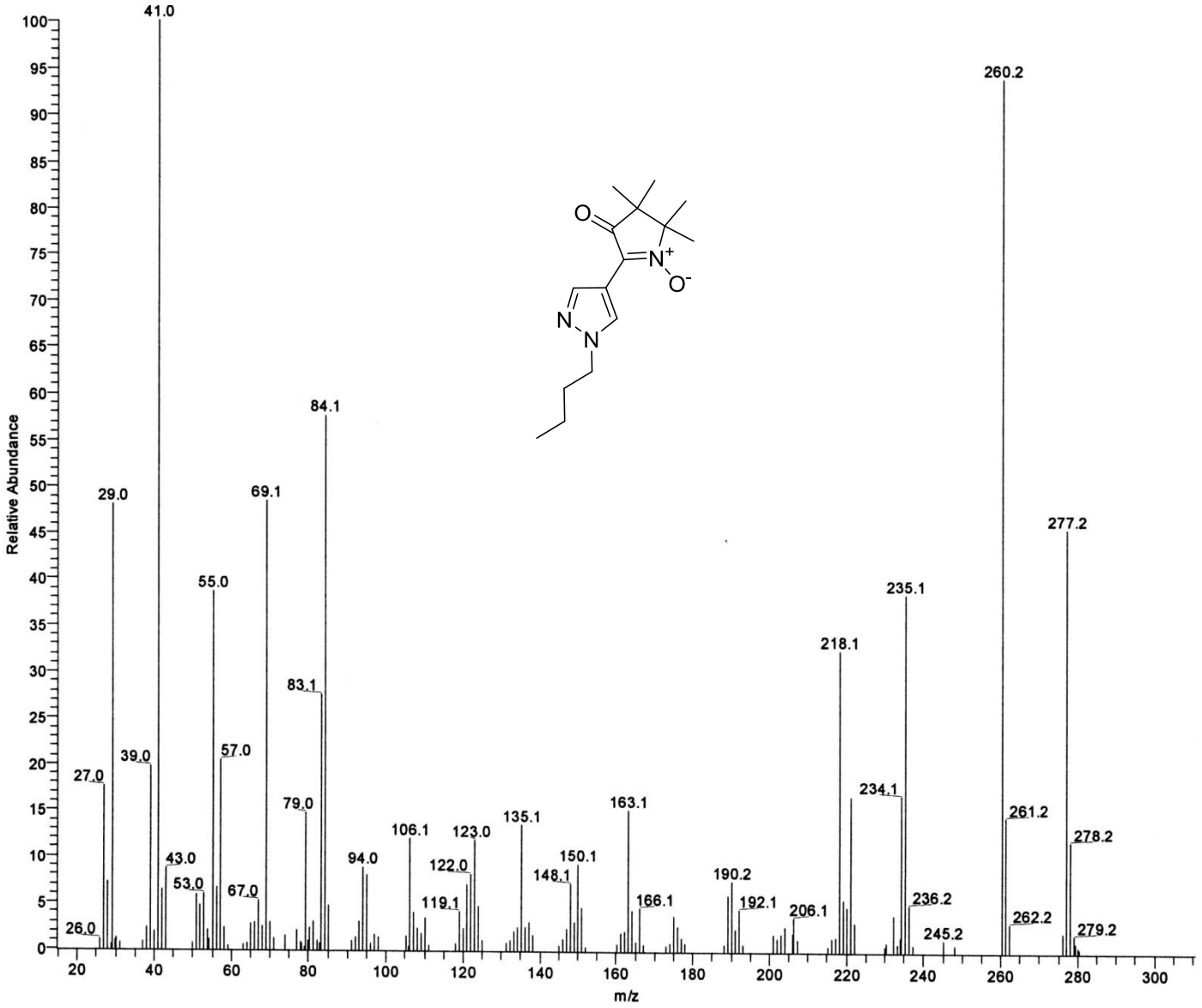
Relative Abundance
m/z
41.0
260.2
84.1
29.0
69.1
277.2
55.0
235.1
218.1
83.1
39.0
57.0
27.0
234.1
79.0
163.1
261.2
106.1
123.0
135.1
278.2
43.0
94.0
150.1
122.0
148.1
190.2
53.0
67.0
166.1
192.1
236.2
119.1
206.1
262.2
26.0
245.2
279.2
O
N+
O-
N
N

IR Spectra of NN^{Alk}, and Comparison of IR Spectra of NN^{Alk} (Alk = Me, Et) and 4a,b

2-(1-Methyl-1H-pyrazol-4-yl)-4,4,5,5-tetramethyl-4,5-dihydro-1H-imidazole-3-oxide-1-oxyl (NN^{Me})

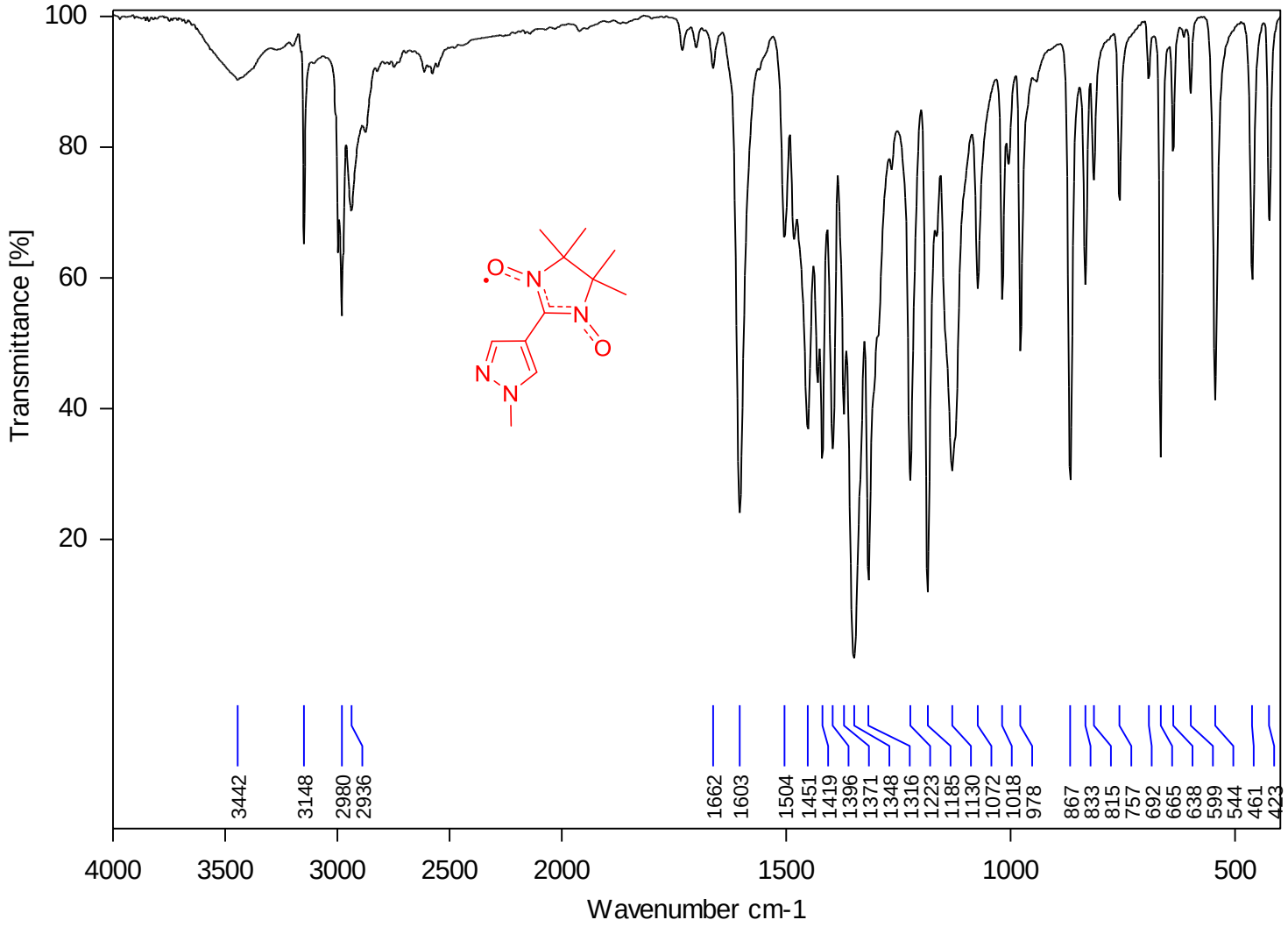

*2-(1-Ethyl-1H-pyrazol-4-yl)-4,4,5,5-tetramethyl-4,5-dihydro-1H-imidazole-3-oxide-1-oxyl (**NN^{Et}**)*

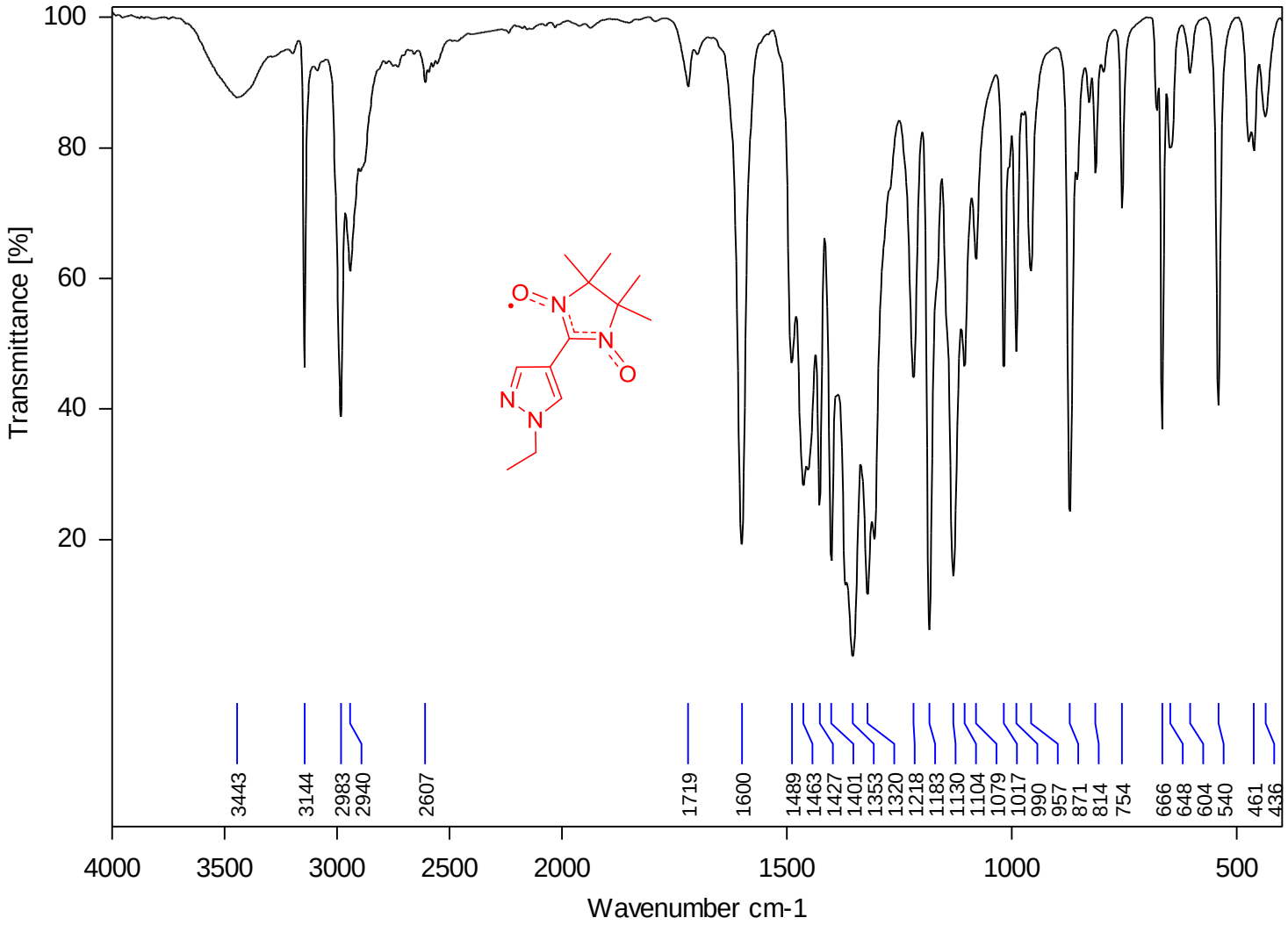

*2-(1-n-Propyl-1H-pyrazol-4-yl)-4,4,5,5-tetramethyl-4,5-dihydro-1H-imidazole-3-oxide-1-oxyl (**NN^{Pr}**)*

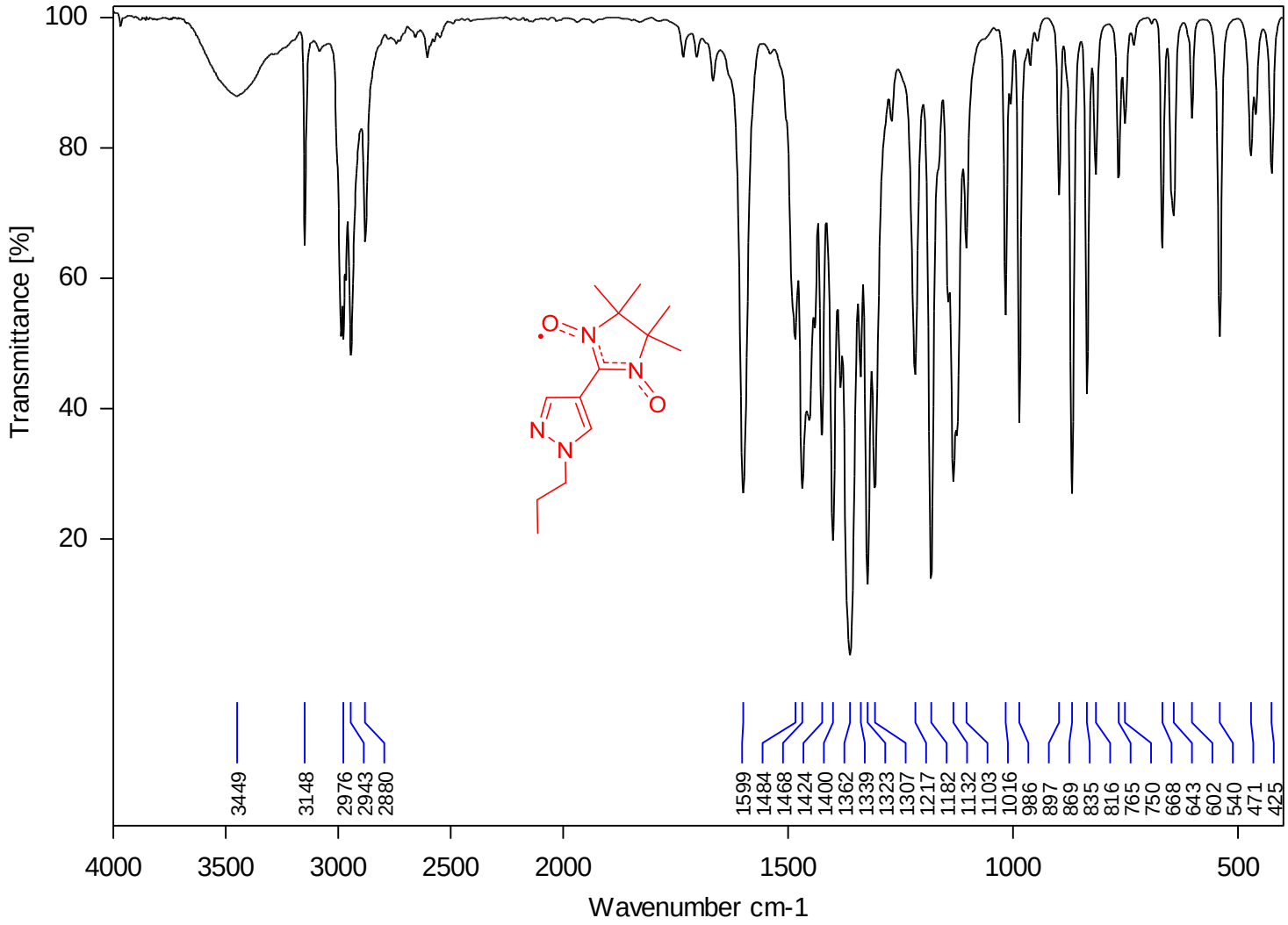

*2-(1-n-Butyl-1H-pyrazol-4-yl)-4,4,5,5-tetramethyl-4,5-dihydro-1H-imidazole-3-oxide-1-oxyl (**NN^{Bu}**)*

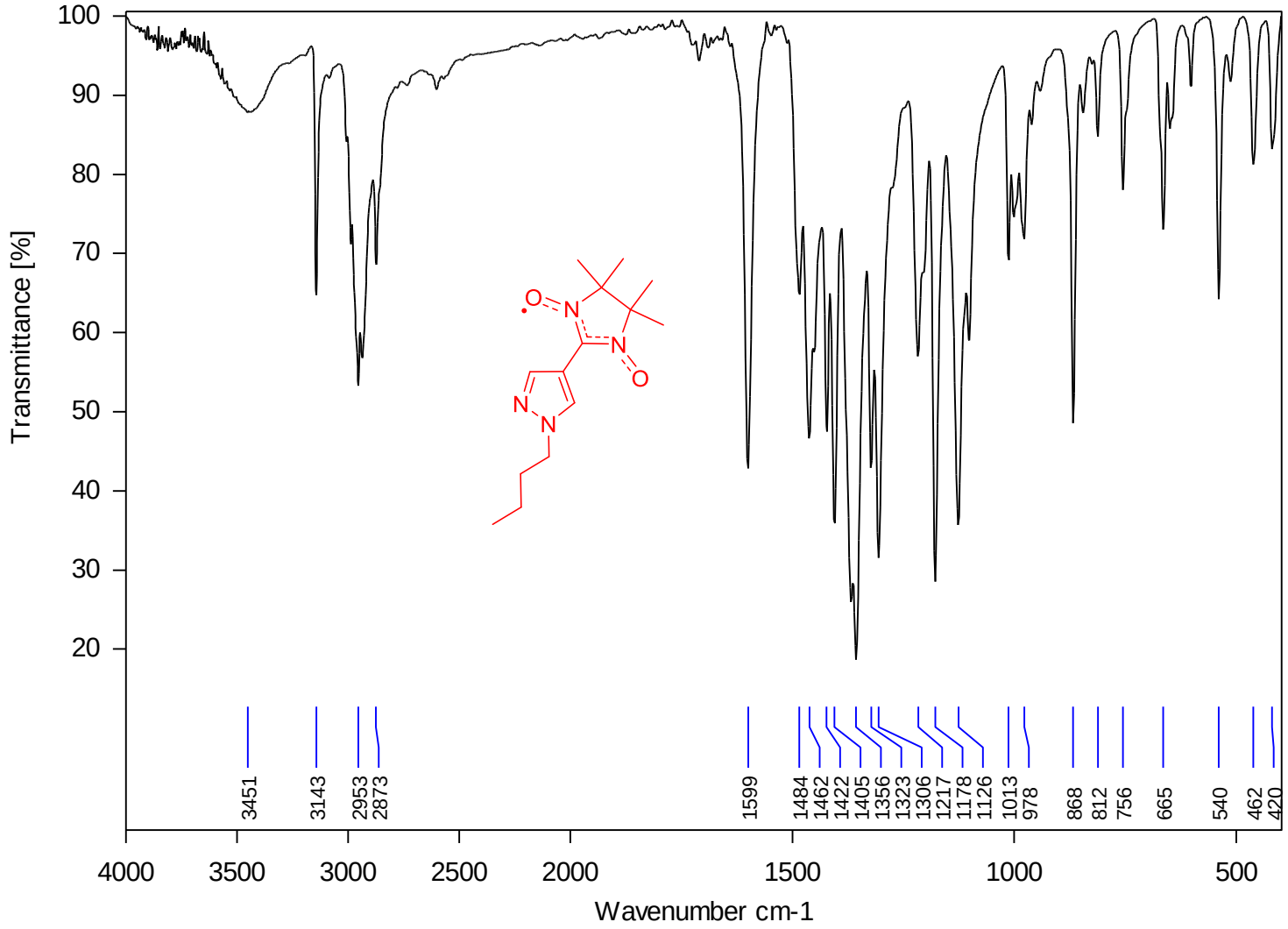

*Shifted relative to each other the IR spectra of 2,2,3,3-tetramethyl-5-(1-methyl-1H-pyrazol-4-yl)-4-oxo-3,4-dihydro-2H-pyrrole 1-oxide (**4b**) and 2-(1-methyl-1H-pyrazol-4-yl)-4,4,5,5-tetramethyl-4,5-dihydro-1H-imidazole-3-oxide-1-oxyl (**NN^{Et}**)*

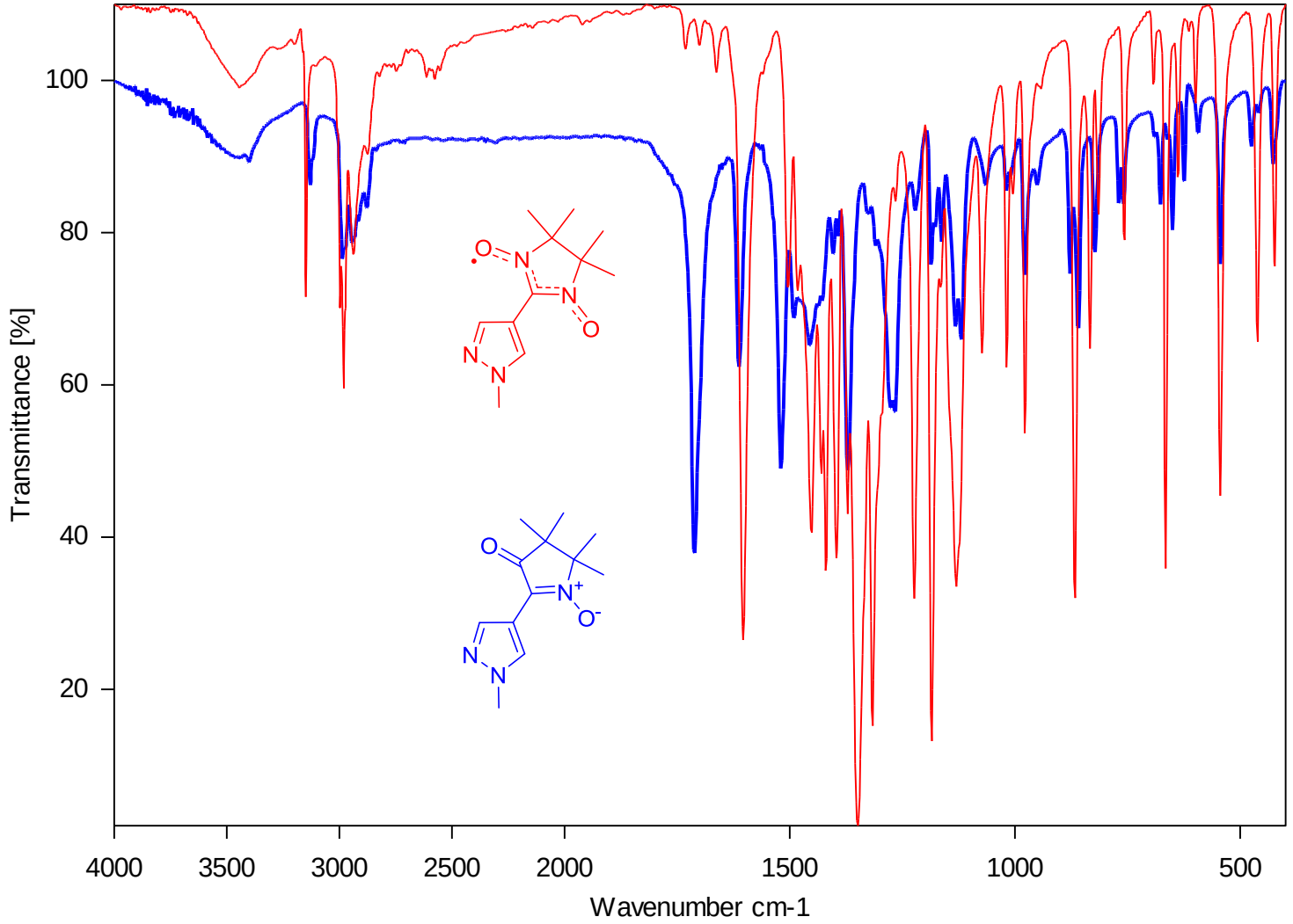

*Shifted relative to each other the IR spectra of 2,2,3,3-tetramethyl-5-(1-ethyl-1H-pyrazol-4-yl)-4-oxo-3,4-dihydro-2H-pyrrole 1-oxide (**4b**) and 2-(1-ethyl-1H-pyrazol-4-yl)-4,4,5,5-tetramethyl-4,5-dihydro-1H-imidazole-3-oxide-1-oxyl (**NN^{Et}**)*